

Garnet-bearing tonalitic porphyry from East Kunlun, Northeast Tibetan Plateau: implications for adakite and magmas from the MASH Zone

Chao Yuan · Min Sun · Wenjiao Xiao · Simon Wilde · Xianhua Li · Xiaohan Liu · Xiaoping Long · Xiaoping Xia · Kai Ye · Jiliang Li

Received: 15 November 2007 / Accepted: 1 June 2008 / Published online: 25 June 2008
© Springer-Verlag 2008

Abstract A garnet-bearing tonalitic porphyry from the Achiq Kol area, northeast Tibetan Plateau has been dated by SHRIMP U-Pb zircon techniques and gives a Late Triassic age of 213 ± 3 Ma. The porphyry contains phenocrysts of Ca-rich, Mn-poor garnet ($\text{CaO} > 5$ wt%; $\text{MnO} < 3$ wt%), Al-rich hornblende ($\text{Al}_2\text{O}_3 \sim 15.9$ wt%), plagioclase and quartz, and pressure estimates for hornblende enclosing the garnet phenocrysts yield values of 8–10 kbar, indicating a minimum pressure for the garnet. The rock has SiO_2 of 60–63 wt%, low MgO (<2.0 wt%), K_2O (<1.3 wt%), but high Al_2O_3 (>17 wt%) contents, and is metaluminous to slightly peraluminous ($\text{ACNK} = 0.89$ –1.05). The rock samples are enriched in LILE and LREE but depleted in Nb and Ti, showing typical features of subduction-related magmas. The relatively high Sr/Y (~38) ratios and low HREE ($\text{Yb} < 0.8$ ppm) contents suggest that garnet is a residual phase, while suppressed crystallization of plagioclase and lack of negative Eu anomalies indicate a high water fugacity in the magma.

C. Yuan (✉) · X. Li · X. Long
Key Laboratory of Isotope Geochronology and Geochemistry,
Guangzhou Institute of Geochemistry, Chinese Academy
of Sciences, Guangzhou 510640, China
e-mail: yuanchao@gig.ac.cn

M. Sun · X. Xia
Department of Earth Sciences, The University of Hong Kong,
Pokflam Road, Hong Kong, China

W. Xiao · X. Liu · K. Ye · J. Li
State Key Laboratory of Lithospheric Evolution,
Institute of Geology and Geophysics, Chinese Academy
of Sciences, Beijing 100029, China

S. Wilde
Department of Applied Geology, Curtin University
of Technology, Perth, Australia

Nd–Sr isotope compositions of the rock ($\epsilon_{\text{Nd}_T} = -1.38$ to -2.33 ; $^{87}\text{Sr}/^{86}\text{Sr}_i = 0.7065$ – 0.7067) suggest that both mantle- and crust-derived materials were involved in the petrogenesis, which is consistent with the reverse compositional zoning of plagioclase, interpreted to indicate magma mixing. Both garnet phenocrysts and their ilmenite inclusions contain low MgO contents which, in combination with the oxygen isotope composition of garnet separates (+6.23‰), suggests that these minerals formed in a lower crust-derived felsic melt probably in the MASH zone. Although the rock samples are similar to adakitic rocks in many aspects, their moderate Sr contents (<260 ppm) and La/Yb ratios (mostly 16–21) are significantly lower than those of adakitic rocks. Because of high partition coefficients for Sr and LREE, fractionation of apatite at an early stage in the evolution of the magma may have effectively decreased both Sr and LREE in the residual melt. It is suggested that extensive crystallization of apatite as an early phase may prevent some arc magmas from evolving into adakitic rocks even under high water fugacity.

Keywords Garnet · Adakite · MASH Zone · Kunlun · Tibetan Plateau

Introduction

Convergent plate boundaries, also known as the “subduction factory”, are very important for crustal growth and material recycling (Tatsumi and Eggins 1995; Stern 2002). Arc magmas, as a product of subduction, retain important clues of the energy and material transfer between mantle and crust, and the crust-mantle transition zone commonly plays a crucial role in crust-mantle interactions. Due to negative

buoyancy, mantle-derived magma commonly pools at the crust-mantle transition zone and interacts with crustal materials, causing extensive mixing, assimilation, storage and homogenization (MASH) (Hildreth and Moorbath 1988; Dufek and Bergantz 2005; Annen et al. 2006; Lee et al. 2006; Tassara 2006; Berger et al. 2007). In active continental margin and mature arc systems, the MASH zone is generally at a depth corresponding to the garnet stability field (ca. 30 km) and mostly around the crust-mantle transition zone. Differentiation of primary magma in the MASH zone will leave garnet pyroxenite cumulates, which may subsequently sink into the mantle by delamination and cause mantle heterogeneity (van Sestrenen et al. 2001; Anderson 2006; Behn and Kelemen 2006). A largely neglected and perhaps equally important aspect is residual melt from the MASH zone. Recently, a high pressure differentiation regime for arc magmas in the garnet stability field has been invoked to explain the occurrence of adakites with normal geothermal gradients (e.g., Macpherson et al. 2006; Richards and Kerrich 2007; Roderíguez et al. 2007). If these authors are correct, the question arises why only a small amount of arc magma can finally evolve into adakite in normal subduction zones or, alternatively, what happened to those non-adakitic arc magmas during their differentiation. The MASH zone therefore becomes a key factor for understanding magmatic evolution and crustal growth. Fossil arc sections and mafic-ultramafic xenoliths have been investigated to understand the magmatic and geochemical processes in the MASH zone, but these samples generally represent restites or cumulates of magma (Hermann et al. 1997; Greene et al. 2006; Berger et al. 2007; Garrido et al. 2006; Bryant et al. 2007), and samples of residual melt from the MASH zone are still rare.

Although scarce worldwide, garnet-bearing metaluminous intrusions have been found in some subduction-related environments, e.g., Northland, New Zealand, northern Pannonian Basin in eastern-central Europe and Setouchi Volcanic Belt in Japan (Day et al. 1992; Harangi et al. 2001; Nitoi et al. 2002; Bandrés et al. 2004; Kawabata and Takafuji 2005). In contrast with those in S-type granitic plutons, garnet in metaluminous intrusions is characterized by Ca-rich, Mn-poor almandine and generally forms under relatively high pressure conditions, mostly corresponding to the depth of the crust-mantle transition zone (Day et al. 1992; Green 1992). Rapid ascent of the garnet-bearing magma under an extensional regime and with high volatile content, effectively prevents garnet crystals from being dissolved during subsequent re-equilibrium under low pressure conditions (Day et al. 1992; Harangi et al. 2001). Therefore, garnet-bearing metaluminous rocks may represent intact melt from the base of the crust and provide a rare opportunity to evaluate magmatic and geochemical processes in the MASH zone.

This paper reports SHRIMP U-Pb zircon results and geochemical data for a garnet-bearing tonalite porphyry from East Kunlun, at the northeastern margin of the Tibetan Plateau. The geochemical results, together with petrographic observations and mineral analyses, also shed light on the genesis of adakitic rocks in general.

Geological background

The Tibetan Plateau is comprised of micro-continental and arc-derived blocks and at least five suture zones have been identified in the plateau, indicating a multiple orogenic history (Chang et al. 1986; Dewey et al. 1988; Pan et al. 1996; Matte et al. 1996; Sobel and Arnaud 1999; Yin and Harrison 2000; Xiao et al. 2002a, b; Cowgill et al. 2003; Gehrels et al. 2003a, b; Schwab et al. 2004; Yuan et al. 2005). The Kunlun Mountain range extends for more than 2,500 km along the northern margin of the Tibetan Plateau and records the earliest collage history of the plateau (Fig. 1). It is cut by the Altyn Fault, which divides the Kunlun Mountains into West and East sections. The East Kunlun consists of three sub-parallel branches, i.e., Qimantag in the north, Burhanbudashan-Animaqingshan in the middle and Kokoxilishan in the south (Fig. 1). Previous work has revealed that the East Kunlun has undergone at least two orogenies that are closely related to the consumption of the Proto-Tethys (Neoproterozoic to Early Devonian) and Paleo-Tethys (Carboniferous to Jurassic) oceans, respectively (Sengör 1987; Pan et al. 1996; Bian et al. 2004). Ordovician and Carboniferous dismembered ophiolites have been recognized in the East Kunlun (Jiang 1992; Yang et al. 1999; Wang et al. 1999; Lan et al. 2000; Bian et al. 2004), and two episodes of magmatism have also been identified, one in the early Paleozoic (Caledonian) and the other in the Late Paleozoic to early Mesozoic (Indosinian) (Pan et al. 1996; Sobel and Arnaud 1999; Cowgill et al. 2003; Gehrels et al. 2003a, b; Liu et al. 2005). Precambrian basement mainly outcrops in the east part of the East Kunlun (east of 92°E) and is dominated by mid- to late-Proterozoic gneissic rocks (Wang et al. 2004; Chen et al. 2006). Tectonically, the East Kunlun can be subdivided into three belts by the E-W trending South Qimantag Fault and Mid Kunlun Fault along the Burhanbudashan (Jiang 1992) (Fig. 1). The northern belt is characterized by thick Paleozoic (Ordovician to early Carboniferous) clastic and carbonate sediments interlayered with mafic volcanic rocks (Li et al. 2000; Pan et al. 2002). The middle belt is characterized by widespread Neoproterozoic and Late Mesozoic granitic magmatism. Precambrian rocks in this belt exhibit progressively weaker metamorphism, from bottom to top, i.e. from gneiss, schist to weakly metamorphosed carbonate and clastic rocks.

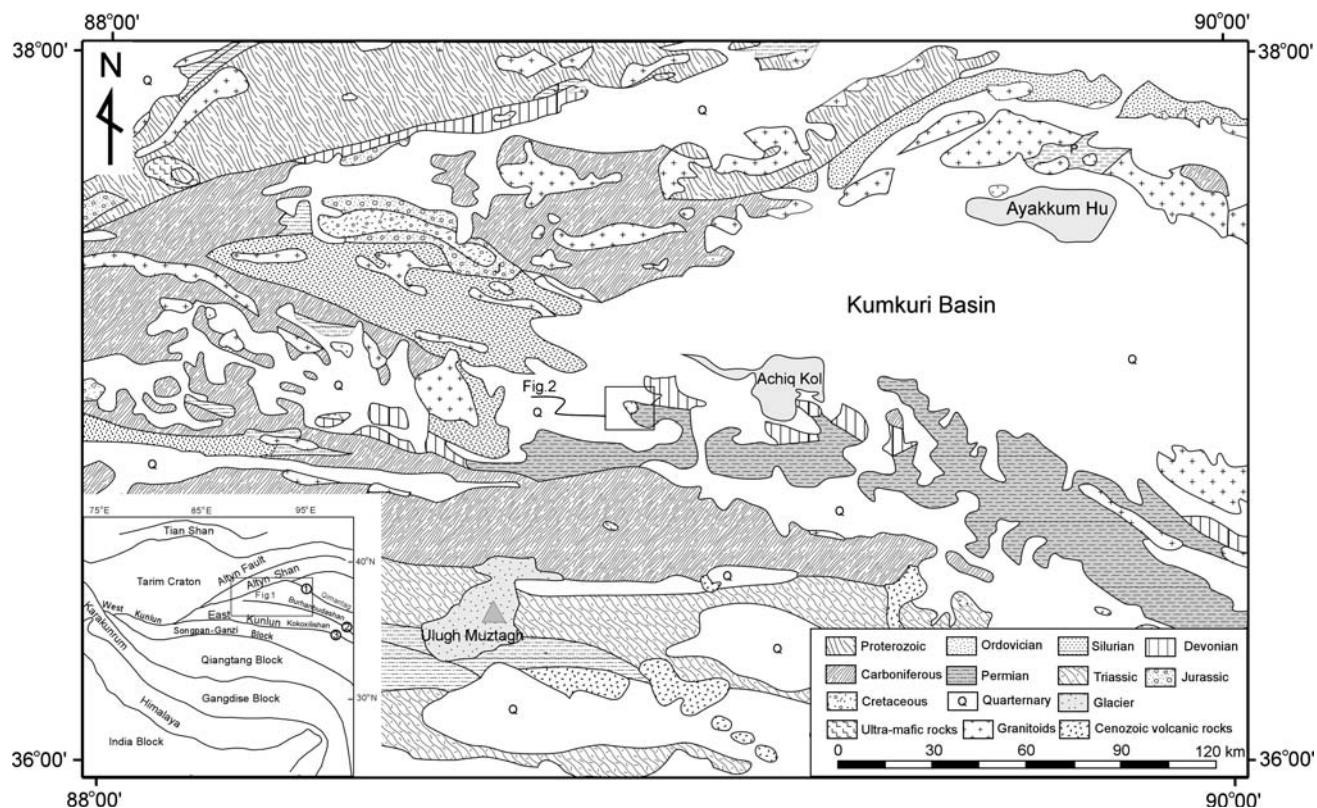


Fig. 1 Geological map of Eastern Kunlun (modified from CIGMR 1988) Inset: tectonic map of the Himalayan-Tian Shan region ① South Qimantag fault; ② Mid Kunlun fault ③ South Kunlun fault

(Jiang 1992). South of the Mid Kunlun Fault, the southern belt is dominated by Precambrian to Jurassic clastic and carbonate rocks. In addition, Lower Carboniferous strata here contain a thick (>3,000 m) mafic to intermediate volcanic sequence, which has been interpreted as having been produced in a subduction environment (Wu et al. 2005). Of the major faults in the East Kunlun, the Mid Kunlun Fault was considered to be a suture zone and the most important geological boundary separating the middle and south Kunlun belts (Jiang 1992). The area underwent continuous tectonism during the Late Paleozoic and Early Mesozoic and this was a key period in the geological evolution of the East Kunlun (Luo et al. 1999), of which the Late Triassic to Jurassic was the most critical period, encompassing the change from compressional to extensional regimes as evidenced by mantle-derived magmatism and hypabyssal intrusions (Qian et al. 2000; Luo et al. 2002). The final closure of Paleo-Tethys occurred in the Jurassic (Sengör 1987; Dewey et al. 1988; Yin and Harrison 2000), with a soft collision proposed to explain the lack of significant crustal thickening in the East Kunlun (Yin and Zhang 1997). After this period, the East Kunlun was relatively stable until the Cenozoic when K-rich volcanism was extensive in the northern Tibetan Plateau (Jiang 1992; Deng 1998; Yang et al. 2002).

An unusual garnet-bearing tonalitic porphyry is located to the west of Achiq Kol, in the Kumkuri area, a Cenozoic basin bounded by the Altyn Fault, and Kunlun and Qimantag mountain ranges (Figs. 1, 2). The basin is mostly filled with Neogene and Quaternary sediments, and Paleozoic strata are only locally exposed, being dominated by Carboniferous to Permian carbonate interlayered with clastic sediments and volcanic rocks (CIGMR 1988). The garnet-bearing tonalitic porphyry is a small, undeformed subvolcanic stock intruding Permian limestone at the northern margin of Burhanbudashan, with an outcrop of ca. 8 km² (Fig. 2).

Rock description and petrography

The garnet-bearing tonalitic porphyry is homogeneous and no enclaves were found. The rock has a porphyritic texture, with garnet, hornblende, plagioclase and quartz set in a cryptocrystalline matrix. Garnet is generally less than 2 mm in size, though some reaches 10 mm in diameter (Fig. 3a). Most garnet is isolated, although some occurs as aggregates (Fig. 3b–d). Garnet is commonly surrounded by plagioclase or hornblende, indicating its early crystallization (Fig. 3b, c). Under the microscope, garnet crystals

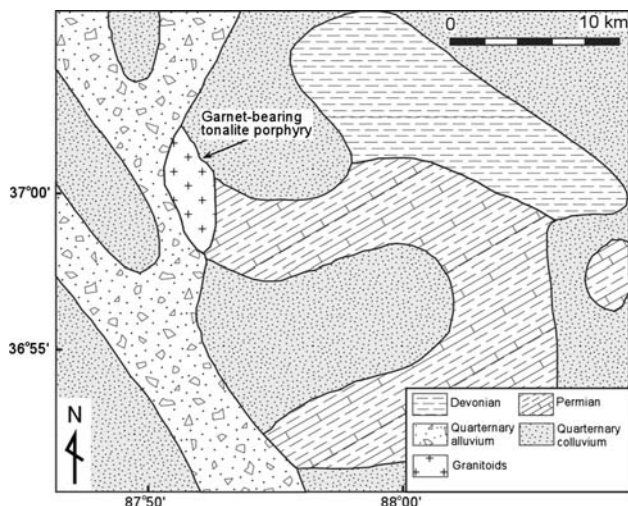


Fig. 2 Geological map of the Achiq Kol area, East Kunlun

are generally euhedral with concentric zoning. Although enveloped in both plagioclase and hornblende, garnet has sharp boundaries without any reaction rim. Small mineral inclusions are common in the garnet and these are dominantly needle-like apatite and ilmenite, with local zircon. Unlike examples from Northland, New Zealand and the northern Pannonian Basin, eastern-central Europe (Day et al. 1992; Harangi et al. 2001), augite, hornblende and plagioclase inclusions are not present in the garnet. Hornblende is the major mafic mineral in the rock with rhomboid shape, and is locally replaced by chlorite (Fig. 3e, f). Plagioclase is euhedral and many grains are altered to kaolin, and only a few have survived alteration and exhibit concentric zoning (Fig. 3g). Quartz is rare and generally anhedral, indicative of relatively late crystallization (Fig. 3h). The occurrence of quartz and lack of pyroxene and biotite make the garnet-bearing tonalitic porphyry distinct from similar rocks described from New Zealand, Europe and Japan. Thin section observation suggests that the minerals in the rock are phenocrysts crystallized from magma, and no garnet xenocrysts were found.

Analytical methods

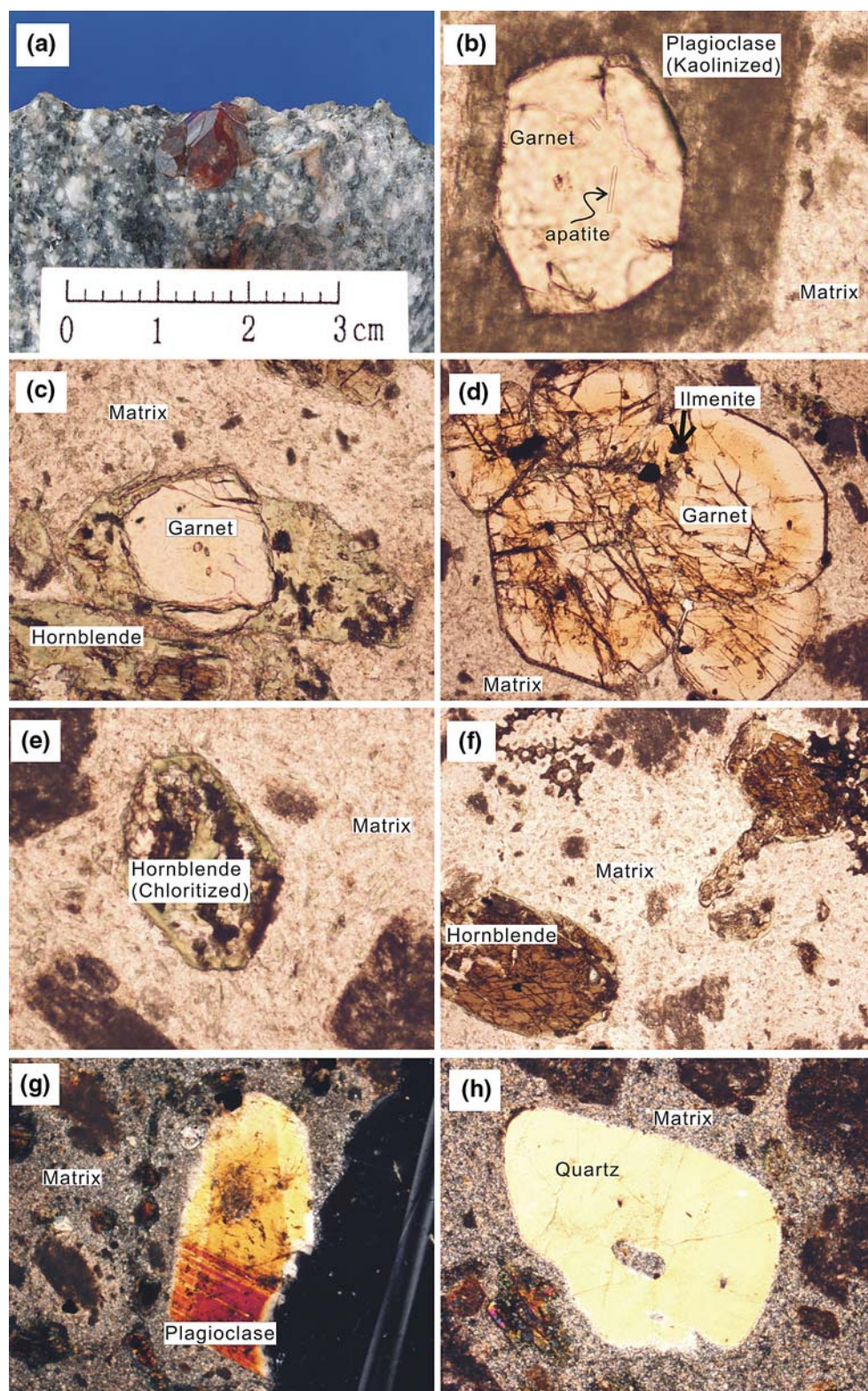
Zircon grains were separated from a sample of garnet tonalite using conventional density and magnetic techniques. Representative zircon grains were hand-picked under a binocular microscope and were cast with pieces of the CZ3 standard in an epoxy mount that was ground to expose the grain centers. U-Th-Pb isotopic compositions were analyzed using the WA Consortium SHRIMP II ion microprobe at Curtin University of Technology, following the analytical procedures of Williams (1998). Sri Lankan

gem zircon standard (CZ3) ($^{206}\text{Pb}/^{238}\text{U} = 0.0914$, equivalent to an age of 564 Ma) was used as the standard, and the U and Th decay constants recommended by Steiger and Jäger (1977) were adopted for age calculation. Measured $^{238}\text{U}/^{206}\text{Pb}$ ratios and reported ages have been corrected using the measured ^{204}Pb (Compston et al. 1984). The analytical data were reduced and calculated using the Krill program of P.D. Kinny (Curtin University) and then plotted using the IsoplotEx 2.46 program (Ludwig 2001). Uncertainties on individual analyses are reported at the 1σ level, and mean ages for pooled $^{206}\text{Pb}/^{238}\text{U}$ results are quoted at the 95% confidence level (2σ). Detailed analytical data are given in Table 1, and the concordia plots are presented in Fig. 4.

Major element composition of the phenocrysts was analyzed using a Cameca SX-51 electron microprobe at the Institute of Geology and Geophysics, Chinese Academy of Sciences. The acceleration voltage and beam current were set at 15 kV and 20 nA, respectively. Detailed analytical procedure has been described in Liu and Ye (2004), and both natural and synthetic minerals were used for standard calibration. The analytical errors at 1σ for Na, Mg, Al, Si, K, Na, Ca, Ti, Cr, Mn, Fe, and Ni are generally better than 0.12%. Major oxides of selected whole-rock samples were determined with a Rigaku ZSX100e X-ray fluorescence spectrometer on fused glass disks at the Guangzhou Institute of Geochemistry, Chinese Academy of Sciences (GIGCAS), with analytical uncertainties between 1 and 5%. Trace elements were analyzed using a Perkin-Elmer Scieix ELAN 6000 ICP-MS, following the procedures described by Li (1997). About 50 mg of powdered sample was digested with mixed $\text{HNO}_3 + \text{HF}$ acid in steel-bomb coated Teflon beakers in order to assure complete dissolution of the refractory minerals. Rh was used as an internal standard to monitor signal drift, and the USGS rock standards GSP-1, G-2, W-2 and AGV-1 and the Chinese national rock standards GSR-1 and GSR-3 were analyzed in order to calibrate element concentrations of the unknown samples. Analytical uncertainties were generally better than 5%.

Sr and Nd isotopic analyses were performed on a Finnigan MAT-262 at the Institute of Geology and Geophysics, Chinese Academy of Sciences, following the procedures described by Zhang et al. (2002). Cation columns were used to separate Sr and rare earth elements (REEs), and the REE fraction was further separated with HDEHP-coated Kef columns to obtain Nd. Measured $^{87}\text{Sr}/^{86}\text{Sr}$ and $^{143}\text{Nd}/^{144}\text{Nd}$ ratios were normalized to $^{86}\text{Sr}/^{88}\text{Sr} = 0.1194$ and $^{146}\text{Nd}/^{144}\text{Nd} = 0.7219$, respectively. The reported $^{87}\text{Sr}/^{86}\text{Sr}$ and $^{143}\text{Nd}/^{144}\text{Nd}$ ratios were respectively adjusted to the NBS SRM 987 standard $^{87}\text{Sr}/^{86}\text{Sr} = 0.71025$ and the Shin Etsu JNDI-1 standard $^{143}\text{Nd}/^{144}\text{Nd} = 0.512115$. Oxygen was extracted from a garnet separate using the standard BrF_5 technique (Taylor

Fig. 3 Photographs of rock specimen and major minerals in the garnet-bearing tonalitic porphyry, East Kunlun **(a)** Rock specimen with garnet crystals **(b)** Garnet, with apatite inclusions, enclosed in kaolinized plagioclase (PPL, $\times 40$). **c** Garnet enclosed in chloritized hornblende (PPL, $\times 40$). **d** Garnet aggregate showing concentric zoning and ilmenite inclusion (PPL, $\times 40$). **e** Chloritized hornblende showing idiomorphic crystal form (PPL, $\times 40$). **f** Fresh hornblende phenocryst with 120° cleavages (PPL, $\times 40$). **g** Plagioclase phenocryst with reverse zoning (PPL, $\times 40$). **h** Partly resorbed anhedral quartz phenocryst in fine-grained matrix (PPL, $\times 40$)

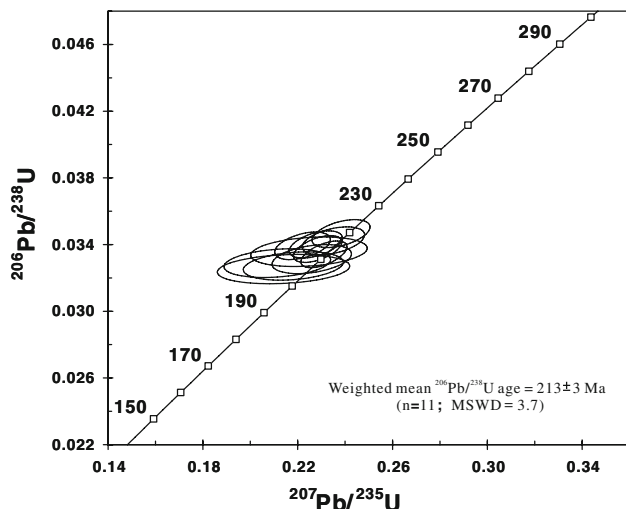


and Epstein 1962). Before analysis, powders were dried at 110°C for 2 h to release adsorbed water. Isotope analyses were performed on a MAT-252 mass spectrometer. The

$^{18}\text{O}/^{16}\text{O}$ ratio is expressed by the conventional $\delta^{18}\text{O}$ notation in permil relative to V-SMOW. The analytical error of $\delta^{18}\text{O}$ values is $\pm 0.1\text{\textperthousand}$.

Table 1 SHRIMP zircon U–Pb results for the garnet-bearing tonalitic porphyry, East Kunlun

Spot name	U ppm	Th ppm	Th/U	$^{207}\text{Pb} / ^{206}\text{Pb}$	%err	$^{207}\text{Pb} / ^{235}\text{U}$	%err	$^{206}\text{Pb} / ^{238}\text{U}$	Error (%)	Error correlation	Age (Ma)				
				*		*		*			$^{206}\text{Pb} / ^{238}\text{U}$	1σ	$^{207}\text{Pb} / ^{206}\text{Pb}$	1σ	
L121.1	440	30	0.07	0.0466		4.21	0.2114	4.35	0.0329	1.07	0.25	209	2	30	101
L122.1	398	31	0.08	0.0486		4.33	0.2248	4.47	0.0336	1.08	0.24	213	2	127	102
L123.1	939	308	0.33	0.0499		1.85	0.2383	2.09	0.0347	0.99	0.47	220	2	188	43
L124.1	369	26	0.07	0.0495		2.83	0.2259	3.03	0.0331	1.07	0.35	210	2	169	66
L125.1	453	80	0.18	0.0484		3.81	0.2181	3.96	0.0327	1.06	0.27	208	2	117	90
L126.1	337	79	0.24	0.0477		5.22	0.2140	5.33	0.0325	1.10	0.21	206	2	85	124
L127.1	1146	235	0.21	0.0502		1.41	0.2311	1.72	0.0334	0.98	0.57	212	2	202	33
L128.1	837	156	0.19	0.0475		1.92	0.2220	2.16	0.0339	0.99	0.46	215	2	73	46
L129.1	1329	264	0.20	0.0491		1.54	0.2284	1.82	0.0337	0.97	0.53	214	2	153	36
L1210.1	793	192	0.24	0.0498		2.05	0.2350	2.28	0.0342	1.00	0.44	217	2	186	48
L1211.1	1142	275	0.24	0.0485		1.75	0.2276	2.01	0.0340	0.98	0.49	216	2	126	41

**Fig. 4** SHRIMP zircon U–Pb concordia diagrams for the garnet-bearing tonalitic Porphyry, East Kunlun

Geochronology

Zircon grains from the garnet-bearing tonalite porphyry are euhedral and transparent, and generally colorless or light brown. Most grains exhibit concentric oscillatory zoning and no inherited zircon cores were observed. Eleven zircons were analyzed for U–Pb isotopic composition and the results are listed in Table 1. The zircons show a wide range of U (337–1329 ppm) and Th (26–308 ppm) contents. Except for three grains with relatively low Th/U ratios (ca. 0.07), most zircons have moderate Th/U ratios (0.18–0.33), which, together with their internal concentric zoning, indicate a magmatic origin. These analyses form a coherent group with a weighted mean $^{206}\text{Pb} / ^{238}\text{U}$ age of 213 ± 3 Ma (Fig. 4). This age is interpreted as the crystallization age of the rock.

Geochemical results

Mineral compositions

Garnet

Representative compositions of garnet in the tonalite porphyry are listed in Table 2. All garnets have a relatively homogeneous composition, consisting mainly of almandine (56–76 mol%) and grossular (24–30 mol%), with minor pyrope (9–18 mol%) and spessartine (1–7 mol%) components. Although the garnets generally show compositional zoning (Fig. 3a–c), there is no regular compositional variation within the grains. As revealed in Table 2, some garnet shows an increase in MgO, MnO and/or CaO towards the rim, whereas others show the reverse trend. These features are similar to those of garnet phenocrysts in the northern Pannonian Basin, eastern-central Europe and Setouchi, Japan (Harangi et al. 2001; Kawabata and Takafuji 2005). The compositional variation of garnet can be illustrated with a profile analysis on a single garnet crystal (Fig. 5). The components of garnet generally keep relatively constant in the central part of the crystal except for grossular showing a weak fluctuation, although a significant increase in almandine and a decrease in grossular can be observed in the rim, while pyrope and spessartine exhibit only weak variation.

Hornblende

Compositions of representative hornblende crystals are given in Table 3. Hornblende in the garnet-bearing tonalitic porphyry has relatively homogeneous composition. In comparison with those from garnet-bearing andesite from Northland, New Zealand (Day et al. 1992), hornblende in this study is characterized by relatively low MgO (8.81–10.1 wt%), TiO₂ (0.88–1.87 wt%) and CaO

Table 2 Representative major element composition of garnet in the garnet-bearing tonalitic porphyry, East Kunlun

Sample	G-12a1		G-12a2		G-12a3		G-12c-1		G-12c-3		G-a-2	
	Core	Rim	Core	Rim	Core	Mantle	Core	Rim	Core	Mantle	Core	Rim
SiO ₂	37.85	38.48	38.33	37.91	37.86	38.13	38.36	38.17	38.14	38.02	38.1	37.79
TiO ₂	0.62	0.30	0.10	0.19	0.46	0.51	0.20	0.29	0.41	0.32	0.28	0.22
Al ₂ O ₃	20.55	21.46	21.65	21.32	21.20	21.28	21.46	21.03	21.18	21.03	21.18	21.19
Cr ₂ O ₃	—	—	—	—	0.04	0.01	—	—	0.01	0.03	—	—
Fe ₂ O ₃	0.60	0.04	—	0.06	—	—	0.40	0.30	0.27	0.17	0.08	0.14
MgO	2.51	4.33	4.02	3.46	2.87	3.17	3.34	4.22	4.25	3.99	3.69	3.72
CaO	6.24	6.33	5.89	6.03	7.78	7.80	5.95	6.16	7.14	6.92	5.83	5.27
MnO	2.55	1.57	2.44	2.19	2.25	1.76	2.22	1.78	1.48	1.79	1.51	1.82
FeO	29.77	28.14	28.20	29.29	27.82	27.80	29.35	27.74	27.16	27.87	28.00	28.75
NiO	0.03	—	—	—	—	—	0.02	—	0.01	0.02	0.01	0.03
Na ₂ O	0.03	0.03	0.04	0.04	0.04	0.02	0.03	0.02	0.03	0.01	0.01	0.02
K ₂ O	—	—	—	—	—	—	0.01	—	0.01	—	0.02	—
Total	100.75	100.69	100.67	100.49	100.27	100.51	100.95	99.94	99.98	99.62	99.77	99.74
Formular (cations are calculated based on 12 oxygens)												
Si	6.0083	6.0154	6.0097	5.9908	5.9890	5.9997	6.0253	6.0385	6.0070	6.0369	6.0167	5.9781
Ti	0.0743	0.0351	0.0117	0.0221	0.0551	0.0600	0.0234	0.0341	0.0315	0.0349	0.0486	0.0386
Al	3.8447	3.9543	3.9998	3.9710	3.9528	3.9465	3.9721	3.9059	3.9288	3.9222	3.9226	3.9384
Cr	—	—	0.0006	—	—	0.0046	0.0012	—	—	—	0.0018	0.0032
Fe	0.0720	0.0043	—	0.0077	—	0.0000	—	0.0476	0.0353	0.0322	0.0200	0.009
Mg	0.5938	1.0094	0.9405	0.8154	0.6770	0.7429	0.7827	0.9115	0.9975	0.9422	0.8697	0.8778
Ca	1.0610	1.0600	0.9886	1.0203	1.3187	1.3151	1.0010	1.0396	1.2039	1.0445	1.1727	0.9899
Mn	0.3429	0.2085	0.3237	0.2929	0.3009	0.2352	0.2959	0.2375	0.1968	0.2399	0.2026	0.2442
Fe	3.9530	3.6789	3.6974	3.8715	3.6804	3.6583	3.8552	3.6557	3.5744	3.6893	3.7063	3.8097
Ni	0.0043	—	—	0.0004	—	—	0.0026	—	0.0015	0.0026	0.0017	0.0041
Na	0.0096	0.0088	0.0128	0.0113	0.0112	0.0049	0.0090	0.0057	0.0098	0.0031	0.0063	0.0078
K	—	—	—	—	—	—	0.0018	—	0.0027	—	0.0032	—
Total	15.9639	15.9746	15.9848	16.0034	15.9851	15.9672	15.9701	15.9506	15.9823	15.9573	15.9649	15.9513
Uv	—	—	0.01	—	0.12	0.03	—	—	—	0.05	0.08	—
Ad	2.96	0.64	0.18	0.52	0.83	0.91	0.36	1.73	1.37	1.25	0.82	0.92
Gr	14.25	16.86	16.32	16.3	20.8	20.59	16.28	15.53	18.54	16.01	18.06	15.53
Py	10.05	17.01	15.83	13.62	11.39	12.56	13.22	16.79	16.75	15.98	14.69	14.88
Sp	5.81	3.51	5.45	4.89	5.06	3.98	5.00	4.02	3.31	4.07	3.42	4.14
Al	66.93	61.98	62.21	64.67	61.92	61.84	65.11	61.92	60.04	62.58	64.59	64.17

Table 2 continued

Sample	G-a-1			G-c-5			G-c-3			G-c-1			G-5a-1			G-5a-2		
	Core	Mantle	Rim	Core	Mantle	Rim	Core	Rim	Mantle	Rim	Core	Rim	Core	Mantle	Rim	Core	Mantle	Rim
SiO ₂	38.45	37.86	37.95	38.64	38.26	38.61	38.99	38.44	38.02	37.30	38.20	37.60	38.15	37.64	37.98	37.98	37.98	
TiO ₂	0.79	0.16	0.16	0.58	0.56	0.19	0.26	0.25	0.24	0.16	0.08	0.23	0.20	0.18	0.45	0.19	0.19	
Al ₂ O ₃	21.13	21.43	21.28	21.57	21.29	21.53	21.56	21.98	21.70	22.02	21.57	21.71	21.76	21.60	21.56	21.55	21.55	
Cr ₂ O ₃	—	—	—	—	—	—	—	—	—	—	—	—	0.04	—	—	—	—	
Fe ₂ O ₃	0.19	—	0.17	—	0.12	—	—	—	—	—	—	—	—	—	—	—	—	
MgO	3.14	3.62	3.63	2.66	2.65	3.77	4.20	4.50	3.81	4.27	4.13	4.13	3.67	4.28	3.20	3.82	3.82	
CaO	10.74	6.34	5.89	11.25	11.41	6.40	6.99	7.31	5.97	6.23	6.56	6.20	6.41	6.01	7.50	6.48	6.48	
MnO	1.13	1.80	1.99	0.40	0.47	1.61	1.80	1.39	1.85	1.89	1.65	1.63	1.76	1.81	1.76	1.60	1.60	
FeO	25.49	28.93	29.31	26.25	25.68	28.62	27.20	26.71	28.74	28.11	27.95	28.65	28.70	28.70	28.62	28.77	28.77	
NiO	0.03	—	0.01	0.02	—	0.05	—	—	0.02	—	—	0.02	—	—	—	0.01	0.01	
Na ₂ O	0.01	0.05	0.05	0.05	0.05	0.08	0.05	0.03	0.02	0.01	0.05	0.02	0.02	0.03	—	0.03	—	
K ₂ O	—	0.04	—	0.05	0.03	0.04	—	—	—	—	—	—	—	—	—	—	—	
Total	101.10	100.23	100.43	100.78	100.89	100.55	100.67	101.16	100.79	100.69	99.29	100.77	100.17	100.76	100.74	100.44	100.44	
Formular (cations are calculated based on 12 oxygens)																		
Si	5.9863	5.9849	5.9956	5.99405	6.0213	6.0104	6.0256	6.0259	6.0175	5.9503	5.9345	5.9814	0.0241	5.9790	5.9310	5.9797	5.9797	
Ti	0.0931	0.0187	0.019	0.0686	0.0654	0.022	0.030	0.0290	0.0282	0.0188	0.0097	0.0269	0.0530	0.0218	0.0534	0.0230	0.0230	
Al	3.8777	3.9925	3.9617	3.9799	3.9105	3.9861	3.9661	4.0036	4.0032	4.0611	4.0439	4.0057	0.0046	3.9895	4.0042	3.9992	3.9992	
Cr	—	—	—	—	—	—	—	—	—	—	—	—	—	—	—	—	—	
Fe	0.0222	—	0.0198	—	0.0143	—	—	—	—	—	—	—	0.8645	—	—	—	—	
Mg	0.7276	0.8529	0.8544	0.6197	0.6151	0.8825	0.9771	1.0359	0.8880	0.9951	0.9782	0.9632	1.0845	0.9993	0.7522	0.8953	0.8953	
Ca	1.7911	1.0739	0.9973	1.8873	1.9051	1.0771	1.1679	1.2107	1.0010	1.0448	1.1182	1.0408	0.2353	1.0087	1.2669	1.0937	1.0937	
Mn	0.1491	0.2404	0.2662	0.0535	0.0622	0.2137	0.2280	0.1815	0.2457	0.2506	0.2226	0.2159	0.2159	0.2401	0.2342	0.2137	0.2137	
Fe	3.3184	3.8247	3.872	3.4361	3.3469	3.7592	3.5496	3.4522	3.7628	3.6789	3.7190	3.7515	0.0028	3.7613	3.7710	3.7875	3.7875	
Ni	0.0037	—	0.0007	0.0028	—	0.0068	—	—	0.0029	—	0.0006	—	0.0054	—	—	0.0015	0.0015	
Na	0.0030	0.0153	0.0148	0.0153	0.0143	0.0253	0.0140	0.0091	0.0067	0.0018	0.0144	0.0066	—	0.0098	0.0009	0.0085	0.0085	
K	—	0.0089	0.0006	0.0098	0.0057	0.008	—	—	—	—	—	—	16.0084	—	—	—	—	
Total	15.9722	16.0122	16.0023	16.0136	15.9609	15.9912	15.9683	15.9478	15.956	16.0012	16.041	15.9922	—	16.0094	—	16.0139	16.002	
U _V	—	—	—	—	—	—	—	—	—	—	—	—	0.12	—	—	—	—	
Ad	1.97	0.28	0.78	1.04	1.36	0.33	0.46	0.44	0.43	0.28	0.14	0.41	0.36	0.33	0.8	0.35	0.35	
Gr	27.29	17.49	15.71	29.96	30.31	17.64	18.99	19.91	16.3	17.06	18.3	16.8	17.47	16.28	19.81	17.72	17.72	
Py	12.27	14.26	14.29	10.41	10.44	14.91	16.52	17.67	15.1	16.7	16.22	16.17	14.5	16.66	12.55	14.98	14.98	
Sp	2.51	4.02	4.45	0.90	1.06	3.61	4.02	3.09	4.18	4.21	3.69	3.63	3.95	4.00	3.91	3.58	3.58	
Al	55.96	63.95	64.77	57.7	56.82	63.51	60.01	58.88	63.99	61.75	61.65	62.99	63.61	62.73	62.93	63.37	63.37	

Table 2 continued

Sample	G-5c-1		G-5c-2		G-5c-3		G-5c-4		G-2a-3		G-4c-2		G-5b-3		
	Core	Rim	Core	Rim	Core	Rim	Core	Mantle	Core	Rim	Core	Rim	Core	Rim	
SiO ₂	37.79	38.14	37.67	37.87	38.41	38.15	38.10	38.06	38.11	37.88	38.03	37.64	37.31	36.80	38.21
TiO ₂	0.20	0.34	0.17	0.00	0.19	0.00	0.12	0.16	0.18	0.25	0.21	0.23	0.08	0.71	0.19
Al ₂ O ₃	21.70	21.88	22.04	21.78	21.89	21.85	22.07	21.86	21.77	21.84	21.79	21.72	21.55	21.02	21.91
Cr ₂ O ₃	—	—	0.02	—	—	0.02	—	0.02	—	—	0.01	—	—	—	—
Fe ₂ O ₃	—	—	—	—	—	—	—	—	—	—	—	—	—	—	—
MgO	4.07	3.76	3.94	3.73	3.99	4.21	3.86	3.71	3.75	3.80	4.06	3.73	3.20	2.18	4.26
CaO	6.67	6.33	6.96	6.21	7.21	6.45	7.06	6.72	5.85	6.55	6.55	6.69	5.99	7.98	7.69
MnO	1.77	1.71	2.36	1.73	2.37	1.74	2.09	2.23	2.01	1.70	2.30	1.69	2.46	1.99	1.47
FeO	27.85	28.79	27.61	29.11	27.06	28.31	27.93	28.16	29.19	28.72	28.12	28.62	29.80	29.56	27.27
NiO	—	—	—	—	—	0.03	—	0.04	—	0.04	0.01	—	0.01	0.03	0.01
Na ₂ O	—	0.04	0.03	0.02	—	0.01	0.01	0.01	0.01	0.04	0.04	0.05	0.04	0.04	—
K ₂ O	—	—	—	—	—	0.01	—	0.01	—	—	0.02	0.01	—	0.02	0.01
Total	100.06	100.98	100.80	100.46	101.13	100.77	101.23	100.98	100.88	100.82	101.16	100.39	100.44	100.32	101.01
Si	5.9567	5.9663	5.9075	5.9682	5.9815	5.9721	5.9438	5.9611	5.9791	5.9440	5.9451	5.9356	5.9273	5.8842	5.9512
Ti	0.0238	0.0395	0.0199	0.0221	0.0136	0.0136	0.0183	0.0216	0.0290	0.0248	0.0272	0.0098	0.0851	0.0220	—
Al	4.0322	4.0340	4.0735	4.0445	4.0172	4.0310	4.0578	4.0354	4.0262	4.0382	4.0154	4.0378	4.0340	3.9611	4.0221
Cr	—	—	0.0028	—	—	0.0024	—	0.0020	—	—	0.0016	—	—	—	—
Fe	—	—	—	—	—	—	—	—	—	—	—	—	—	—	—
Mg	0.9557	0.8779	0.9221	0.8770	0.9269	0.9821	0.8975	0.8650	0.8777	0.8890	0.9462	0.8772	0.7570	0.5191	0.9891
Ca	1.1272	1.0604	1.1698	1.0491	1.2023	1.0812	1.1809	1.1283	0.9842	1.1009	1.0978	1.1308	1.0193	1.3664	1.2826
Mn	0.2361	0.2263	0.3135	0.2307	0.3128	0.2312	0.2756	0.2963	0.2666	0.2257	0.3049	0.2258	0.3314	0.2698	0.1934
Fe	3.6710	3.7674	3.6214	3.8368	3.5243	3.7057	3.6435	3.6877	3.8293	3.7692	3.6760	3.7750	3.9587	3.9525	3.5523
Ni	—	—	—	—	—	0.0037	—	0.0048	—	0.0053	0.0017	—	0.0019	0.0036	0.0017
Na	0.0009	0.0106	0.0079	0.0058	0.0013	0.0022	0.0022	0.0031	0.0031	0.0124	0.0128	0.0147	0.0128	0.0129	—
K	—	—	—	0.0006	—	0.0014	—	0.0029	—	0.0006	0.0038	0.0029	—	0.0042	0.0024
Total	16.0037	15.9825	16.0384	16.0128	15.9884	16.013	16.0148	16.0049	15.9878	16.0144	16.0299	16.0271	16.0587	16.0169	—
Uv	—	—	0.07	—	—	0.06	—	0.05	—	—	0.04	—	—	—	—
Ad	0.36	0.60	0.30	—	0.33	—	0.20	0.28	0.33	0.44	0.37	0.41	0.15	1.26	0.33
Gr	18.26	16.94	18.88	17.5	19.64	17.96	19.38	18.4	16.01	17.72	17.61	18.19	16.58	20.45	20.81
Py	15.99	14.86	15.33	14.63	15.57	16.37	14.98	14.5	14.76	14.9	15.74	14.64	12.49	8.57	16.47
Sp	3.95	3.83	5.21	3.85	5.25	3.85	4.60	4.97	4.49	3.78	5.07	3.77	5.47	4.45	3.22
Al	61.43	63.76	60.21	64.01	59.2	61.76	60.83	61.81	64.41	63.16	61.16	63.00	65.32	65.26	59.16

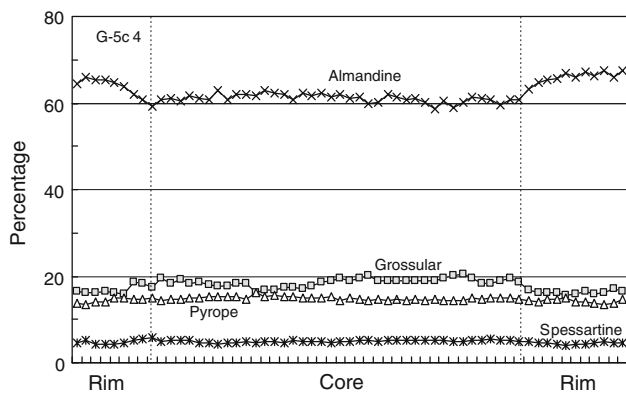


Fig. 5 Line profile of analyses across a representative garnet from the garnet-bearing tonalite porphyry

(10.4–11.2 wt%), and significantly higher Al_2O_3 (12.7–15.9 wt%) and FeO (16.0–17.9 wt%). On the classification diagram, most data plot in the tschermakite field (Fig. 6).

Plagioclase

The representative composition of plagioclase is presented in Table 4. The feldspar is dominated by andesine ($\text{An} = 35\text{--}49$), although one grain is more albite-rich ($\text{An} = 20$). The Or component is generally less than 2%. In comparison with garnet-bearing volcanic rocks of the northern Pannonian Basin, eastern-central Europe (Harangi et al. 2001), plagioclase in this study is relatively poor in Al , Ca and rich in Na , with much lower An values. Significantly, plagioclase generally possesses reversed compositional zoning, with the rims containing a higher proportion of anorthite than the cores (Table 4).

Ilmenite

Ilmenite occurs within garnet phenocrysts, suggesting an early phase of crystallization. The results show that ilmenite is characterized by low MgO (<0.08 wt%) and relatively high MnO (2.08–5.95 wt%) (Table 5). The compositions are in contrast with those of ilmenite in calc-alkaline volcanic rocks of Northland, Stouchi and the northern Pannonian Basin, which is generally Mg-rich ($\text{MgO} > 1$ wt%) and Mn-Poor ($\text{MnO} < 1$ wt%) (Day et al. 1992; Harangi et al. 2001; Kawabata and Takafuji 2005).

Whole-rock geochemistry

Major elements

The whole-rock major and trace element and Nd-Sr isotope compositions of selected samples are presented in Table 6.

The rock samples are homogeneous, with SiO_2 contents ranging from 61.1 to 62.3 wt%. They are low in TiO_2 (<0.5 wt%) and MgO (<2 wt%), and relatively Na-rich with $\text{Na}_2\text{O}/\text{K}_2\text{O}$ ratios between 2.7 and 4.3. The most distinctive feature is the high Al_2O_3 content (17.5–18.1 wt%), consistent with the high proportions of plagioclase and garnet. Despite their relatively high Al_2O_3 contents, most the samples plot in the metaluminous field, except for a few samples showing weakly peraluminous characteristics ($1.0 < \text{ACNK} < 1.1$) (Fig. 7). In the normative feldspar classification diagram, all samples fall in the tonalite field (Fig. 8).

Trace elements

The rock samples have low concentrations of transition elements, e.g., Cr (<20 ppm) and Ni (<13 ppm), compared with rocks with similar SiO_2 in the Andes (e.g., Franchini et al. 2003). Large ion lithophile elements (LILE) and high field strength elements (HFSE) are also relatively low in abundance. Except for the moderate Sr content (208–250 ppm), Rb (35–50 ppm), Cs (1.21–3.27 ppm) and Ba (167–342 ppm) are all relatively low. The contrast between Rb and Sr concentration levels gives rise to the strikingly low Rb/Sr ratios (<0.25). Because of the relatively limited SiO_2 range, most elements do not show definable trends with major oxides (e.g., SiO_2 or MgO). Most HFSE (e.g., Nb , Ta , Zr , Hf) are comparable to those in garnet-bearing I-type granitoids (Day et al. 1992; Harangi et al. 2001) and are comparable or lower than those in felsic magmatic rocks from island arcs (e.g., Mason and McDonald 1978). Like typical rocks at deconstructive plate margins, the samples display LREE-enriched patterns (Fig. 9a), with chondrite-normalized La/Yb ratios between 12 and 38. The distinctive characteristics of the samples are their remarkably low HREE contents ($\text{Yb} = 0.55\text{--}0.73$ ppm) and significant HREE fractionation ($\text{Gd/Yb}_n = 3.2\text{--}5.4$). Most samples have not experienced plagioclase fractionation, because they possess positive Eu anomalies ($\text{Eu/Eu}^* > 1.1$). However, three samples exhibit higher LREE contents and higher La/Yb_n and Gd/Yb_n ratios and slight negative Eu anomalies ($\text{Eu/Eu}^* = 0.85\text{--}0.89$) (Table 5; Fig. 9a). These three samples also show relatively low Zr/Sm ratios (19–24), whereas all other samples have high Zr/Sm ratios (>30), which are different from those of modern mid-ocean-ridge basalts (MORBs), ocean-island basalts (OIB) and island-arc basalts (IAB), but similar to those of Archean TTG and adakitic rocks (Foley et al. 2002). On a primitive mantle normalized spider diagram, the rock is enriched in LILE relative to LREE and HFSE, with pronounced spikes of Pb and troughs of Nb-Ta , P and Ti (Fig. 9b), exhibiting characteristics of typical subduction-related magmas.

Table 3 Representative major element composition of hornblende in the garnet-bearing tonalitic porphyry, East Kunlun

Sample	g12b-4a	g12b-4b	g12c-2ac	g12c-2br	g5a-3c	g5a-3r	g5a-5c	g-5a-5r	g5a-5c	g7a-1r	g7a-1c	g2a-2c	g2a-2b	g2a-2r	g5b-1a	g5b-1b
SiO ₂	42.21	42.82	43.29	43.31	43.41	42.91	41.63	41.92	41.75	42.35	42.97	41.35	44.67	43.47	42.43	41.12
TiO ₂	1.25	0.97	1.13	1.01	1.13	1.08	1.08	0.99	0.94	0.88	0.98	1.87	0.96	1.16	1.07	1.82
Al ₂ O ₃	15.89	15.24	14.32	14.23	14.07	14.53	15.17	15.00	14.86	14.60	14.53	14.97	12.69	14.38	14.04	15.38
Cr ₂ O ₃	0.00	0.01	0.02	0.00	0.04	0.00	0.01	0.01	0.00	0.00	0.00	0.00	0.00	0.00	0.00	0.00
FeO	17.89	17.56	17.85	17.80	16.86	16.45	16.71	16.50	16.89	16.90	17.28	16.09	17.01	17.27	16.87	15.96
MnO	0.11	0.21	0.24	0.25	0.19	0.14	0.19	0.14	0.20	0.33	0.32	0.32	0.24	0.24	0.25	0.29
MgO	8.81	9.10	9.20	9.44	9.42	9.41	8.99	9.21	9.02	8.98	9.26	9.63	10.07	9.29	9.22	9.49
CaO	10.93	11.15	10.82	10.60	11.04	10.97	11.09	10.91	11.04	10.89	10.77	11.11	10.36	10.83	11.04	10.97
Na ₂ O	1.65	1.53	1.60	1.59	1.60	1.59	1.58	1.60	1.61	1.52	1.56	1.96	1.44	1.54	1.47	1.90
K ₂ O	0.56	0.61	0.55	0.59	0.54	0.41	0.58	0.45	0.53	0.56	0.53	0.48	0.35	0.47	0.53	0.48
NiO	0.00	0.00	0.00	0.01	0.04	0.03	0.00	0.00	0.00	0.01	0.01	0.00	0.01	0.01	0.05	0.04
Total	99.31	99.19	99.02	98.82	98.35	97.52	97.02	96.72	96.85	97.01	98.22	97.77	97.79	98.65	96.96	97.44
Formula (cations based on 23 oxygens)																
Si	6.21	6.30	6.38	6.40	6.42	6.38	6.26	6.30	6.29	6.36	6.37	6.17	6.61	6.41	6.38	6.15
Al ^{IV}	1.79	1.70	1.62	1.60	1.58	1.62	1.74	1.70	1.71	1.64	1.63	1.83	1.39	1.59	1.62	1.85
Al ^{VI}	0.970	0.945	0.874	0.872	0.870	0.929	0.944	0.957	0.930	0.945	0.915	0.801	0.826	0.908	0.865	0.856
Ti	0.139	0.107	0.126	0.112	0.126	0.121	0.122	0.112	0.107	0.100	0.109	0.210	0.106	0.128	0.121	0.205
Cr	0.000	0.001	0.002	0.000	0.005	0.000	0.001	0.001	0.000	0.000	0.000	0.000	0.000	0.000	0.000	0.000
Fe ²⁺	2.202	2.161	2.202	2.198	2.085	2.046	2.100	2.074	2.128	2.122	2.144	2.007	2.105	2.130	2.121	1.996
Mn	0.014	0.027	0.030	0.032	0.024	0.018	0.024	0.018	0.026	0.041	0.041	0.040	0.030	0.030	0.032	0.036
Ni	0.000	0.000	0.000	0.001	0.005	0.003	0.000	0.000	0.000	0.001	0.001	0.000	0.001	0.001	0.006	0.004
Mg	1.934	1.996	2.022	2.079	2.078	2.086	2.015	2.063	2.025	2.010	2.048	2.142	2.222	2.041	2.065	2.114
Total	5.258	5.237	5.255	5.293	5.193	5.203	5.206	5.226	5.216	5.219	5.258	5.200	5.291	5.238	5.209	5.212
Ca	1.723	1.758	1.710	1.677	1.749	1.748	1.786	1.757	1.782	1.753	1.713	1.776	1.643	1.711	1.778	1.757
Na	0.018	0.005	0.035	0.030	0.058	0.049	0.008	0.017	0.002	0.028	0.029	0.024	0.066	0.051	0.013	0.031
Total	15.000	15.000	15.000	15.000	15.000	15.000	15.000	15.000	15.000	15.000	15.000	15.000	15.000	15.000	15.000	15.000
Na	0.453	0.431	0.421	0.425	0.400	0.411	0.451	0.449	0.468	0.416	0.420	0.544	0.347	0.389	0.416	0.518
K	0.106	0.114	0.103	0.112	0.102	0.079	0.111	0.086	0.101	0.107	0.100	0.090	0.065	0.087	0.102	0.092
Total	15.559	15.544	15.525	15.537	15.502	15.489	15.562	15.535	15.569	15.522	15.520	15.634	15.413	15.476	15.517	15.610
Total O.	2.601	2.601	2.596	2.592	2.589	2.574	2.547	2.547	2.541	2.549	2.580	2.566	2.586	2.596	2.547	2.561
O.N.	23	23	23	23	23	23	23	23	23	23	23	23	23	23	23	23
Al	2.757	2.643	2.490	2.477	2.451	2.547	2.687	2.657	2.639	2.584	2.540	2.632	2.213	2.499	2.487	2.709
Na	0.471	0.436	0.457	0.455	0.458	0.460	0.459	0.466	0.470	0.444	0.449	0.567	0.413	0.440	0.429	0.549
XMg	0.28	0.29	0.28	0.29	0.30	0.31	0.29	0.30	0.29	0.29	0.29	0.32	0.31	0.29	0.30	0.31
Pressure	10.1	9.6	8.8	8.8	8.7	9.1	9.8	9.6	9.6	9.3	9.1	9.5	7.5	8.9	8.8	9.9

Sr-Nd-O Isotopic compositions

The porphyry possesses relatively homogeneous Sr and Nd isotope compositions, with initial $^{87}\text{Sr}/^{86}\text{Sr}$ ratios and εNd_T values ranging from 0.7065 to 0.7067 and -2.3 to -1.4 , respectively (Table 6). There are no significant trends between incompatible element ratios (e.g., Sr/Y, Zr/Nb, Zr/Sr and Ba/La) with either $^{87}\text{Sr}/^{86}\text{Sr}$ or εNd_T values. In the Nd–Sr isotope correlation diagram, all the data plot in the field of arc magmatism and are quite close to the mantle array (Fig. 10). Analysis of garnet separates from the tonalite porphyry has yielded a $\delta^{18}\text{O}$ value of $+6.23\text{\textperthousand}$, significantly higher than that of garnet from the mantle ($+5.24\text{\textperthousand}$) (Schulze et al. 2001).

Discussion

Origin of garnet in the tonalite porphyry

The origin of garnet in calc-alkaline rocks has been debated for a long time, being variously envisaged as a xenocryst, a phenocryst or a restite phase (Birch and Gleadow 1974; Popov et al. 1982; Gilbert and Rogers 1989). Green (1977, 1992) noticed a close relationship between garnet composition and the P–T conditions of crystallization and recognized that garnet crystallized under relatively high pressure conditions is more Ca-rich and Mn-poor relative to those formed in shallower environments. In the case of the East Kunlun porphyry, all garnet crystals are euhedral

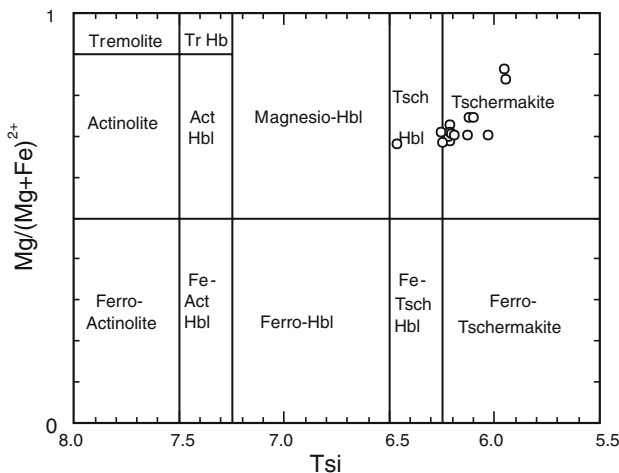


Fig. 6 Classification diagram for hornblende crystals from the garnet-bearing tonalitic porphyry (after Hawthorne 1981)

with concentric zoning and have a similar composition, suggesting a magmatic origin. The data show that all the garnets contain relatively high Ca (CaO = 5.85–11.7 wt%)

and low Mn (MnO = 0.40–2.96 wt%) (Table 2), consistent with crystallization at relatively high pressure (CaO > 4 wt%; MnO < 4 wt%) (Green 1977, 1992; Conrad et al. 1988). In the MnO versus CaO diagram (Fig. 11a), garnets from the tonalite porphyry from East Kunlun show strong affinity to high-pressure garnet. This is different from garnets contained in xenoliths from the Cenozoic volcanic rocks of Hohxil, northern Tibetan Plateau (Deng 1998), which mostly plot in the low-pressure field. The distinctive composition of the garnet is consistent with the petrographic observation and suggests that all the garnets are phenocrysts that crystallized under relatively high pressure. Furthermore, it has been recognized that garnet in cumulates of mantle-derived magma, ecolitic restite and garnet peridotite generally contains high MgO (usually >8 wt%) (e.g., Lee et al. 2006 and references therein). However, garnet in the tonalitic porphyry contains much lower MgO (<4.5 wt%), strikingly different from garnet grown in the mantle environment (Fig. 11b). This may suggest that these garnets crystallized in a felsic, rather than a mafic melt.

Table 4 Representative analyses of plagioclase from the garnet-bearing tonalite porphyry, East Kunlun

Sample	Grt-12c3	Grt-c4c	Grt-c4r	Grt-7a1c	Grt-7a1r	Grt-7a2c	Grt-7a2r	Grt-7a3c	Grt-7a3r
SiO ₂	64.16	57.91	56.73	59.15	57.12	59.54	55.23	59.29	56.48
TiO ₂	–	–	–	–	–	–	0.02	–	–
Al ₂ O ₃	22.92	27.81	28.48	25.92	28.21	26.43	28.11	26.11	28.21
Cr ₂ O ₃	0.21	0.02	0.02	0.01	–	0.02	0.02	0.02	0.01
MgO	–	–	–	–	0.01	–	–	–	–
CaO	3.55	9.07	10.15	7.42	9.64	7.71	10.20	7.56	9.79
MnO	0.02	0.03	0.04	0.05	0.03	0.04	0.04	0.07	0.03
FeO	0.35	0.03	0.07	0.03	0.08	0.02	0.06	0.07	0.05
NiO	0.01	0.03	0.06	–	0.03	–	–	0.01	0.01
Na ₂ O	7.66	6.34	5.85	7.38	6.21	7.15	6.03	7.45	6.19
K ₂ O	0.10	0.21	0.13	0.26	0.15	0.24	0.11	0.23	0.17
Total	98.98	101.45	101.53	100.22	101.48	101.15	99.82	100.81	100.94
Formular (cations based on 8 oxygens)									
Si	2.8404	2.5585	2.5132	2.6366	2.5292	2.6282	2.4945	2.6303	2.517
Ti	–	–	–	–	–	–	0.0006	–	–
Al	1.196	1.4479	1.4866	1.3616	1.4722	1.3751	1.4964	1.3648	1.4817
Cr	0.0073	0.0007	0.0007	0.0004		0.0006	0.0006	0.0007	0.0003
Mg	0.0003	–	–	–	0.0005	–	–	–	–
Ca	0.1683	0.4293	0.4817	0.3542	0.4571	0.3647	0.4934	0.3589	0.4674
Mn	0.0008	0.001	0.0017	0.0018	0.0012	0.0015	0.0014	0.0026	0.0009
Fe	0.0128	0.0011	0.0025	0.0013	0.0029	0.0009	0.0021	0.0026	0.002
Ni	0.0003	0.0011	0.0022	–	0.001	–	–	0.0002	0.0003
Na	0.6577	0.5429	0.5021	0.6378	0.5328	0.6116	0.528	0.6405	0.5352
K	0.0058	0.012	0.0071	0.0149	0.0085	0.0137	0.0065	0.0129	0.0098
Total	4.8897	4.9946	4.9978	5.0087	5.0053	4.9963	5.0236	5.0137	5.0146
ab	79.06	55.16	50.67	63.35	53.37	61.77	51.36	63.27	52.86
or	0.70	1.22	0.72	1.48	0.85	1.38	0.64	1.28	0.96
an	20.23	43.62	48.61	35.18	45.79	36.84	48.00	35.45	46.17

Table 5 Representative composition of ilmenite enclosed in garnet crystals

Sample	Grt-2a-1	Grt-2a-2	Grt-2a-3	Grt-2a-4	Grt-2a-5	Grt-2b-1	Grt-2b-2	Grt-2b-3	Grt-3a-2	Grt-3a-3	Grt-3a-4	Grt-3a-5	Grt-3a-6
SiO ₂	0.02	0.07	0.04	—	0.05	0.04	0.04	0.02	0.04	0.03	0.04	0.06	0.01
TiO ₂	50.47	50.94	50.01	52.26	49.99	49.99	50.78	50.49	50.03	50.84	50.84	49.94	50.17
Al ₂ O ₃	—	0.03	—	0.01	0.10	0.04	0.04	0.07	0.06	0.01	0.02	0.01	0.04
FeO	46.44	43.47	46.90	44.51	44.62	46.39	46.66	45.93	46.01	45.65	45.57	47.02	42.77
MnO	2.56	5.95	2.08	2.66	3.01	2.44	2.43	2.36	2.70	2.98	2.84	2.66	5.02
MgO	0.05	—	0.08	0.02	—	—	0.06	0.06	0.07	0.03	0.03	0.03	0.04
CaO	0.03	0.03	—	0.27	0.21	0.01	—	0.03	0.38	—	—	—	0.01
Na ₂ O	0.03	0.05	0.03	—	0.03	—	0.01	—	0.05	0.04	0.07	—	—
K ₂ O	—	—	—	—	—	—	0.01	—	—	0.01	—	—	—
Cr ₂ O ₃	—	0.01	—	—	0.07	0.05	—	—	0.04	—	—	—	—
Total	99.60	100.55	99.15	99.73	98.09	98.97	100.02	98.97	99.37	99.60	99.41	99.71	98.05

Constraints on the P-T conditions

Several geobarometers and geothermometers have been proposed to estimate the P-T conditions of granitoid batholith formation (e.g., Holland and Blundy 1994; Anderson 1996; Holdaway et al. 1997). Day et al (1992) used phase equilibrium diagrams to constrain the P-T conditions of garnet-bearing andesite in Northland, New Zealand and suggested that the mineral assemblage of garnet + plagioclase + amphibole + quartz is stable around 10 kbar and 800–850°C, and a similar estimate was made for the garnet-bearing calc-alkaline volcanic rocks of the northern Pannonian Basin, eastern-central Europe (Harangi et al 2001). In contrast to multiple mineral barometers, the Al-in-hornblende geobarometer is particularly suitable to estimate the emplacement pressure of granitic rocks (Anderson 1996; Ague 1997). Because garnets in the tonalitic porphyry are mostly surrounded by plagioclase or hornblende, the Al-in-hornblende barometer can provide direct constraint on the crystallization pressure of garnet. Using the Al-in-hornblende barometer calibrated by Schmidt (1992), the pressure is estimated at 7.5–10.1 kbar, suggesting that the garnet crystallized at a crustal depth below 26–35 km. Using the zircon saturation thermometer (Watson and Harrison 1983), the temperature of the tonalite porphyry was estimated as 706–713°C, representing the temperature when the magma was emplaced at a shallower crustal level.

Petrogenesis of the garnet-bearing tonalite porphyry

The relatively high SiO₂, low MgO, Cr and Ni contents suggest an evolved magmatic composition for the garnet-bearing tonalitic porphyry. The relatively high pressure of hornblendes indicates that the phenocrysts formed prior to emplacement of the magma, therefore their compositions may be useful to infer the origin of the early melt. Garnet

phenocrysts with ilmenite inclusions are the earliest phases preserved in the tonalite porphyry. The garnet phenocrysts are compositionally distinct from those crystallized from primary mantle-derived magma and therefore probably formed in an evolved magma (Fig. 11b). Likewise, ilmenite within garnet phenocrysts has a very low MgO (<0.08 wt%) content, much lower than ilmenite in the garnet-bearing andesite/dacite of Northland, New Zealand (1.79–2.48 wt%), northern Pannonian Basin (0.85–3.27 wt%) and the Setouchi volcanic belt (1–1.02 wt%) (Day et al. 1992; Harangi et al. 2001; Kawabata and Takafuji 2005). In addition, the garnet phenocrysts have an oxygen isotope composition (+6.23‰) significantly higher than that of normal mantle-derived garnets (+5.24‰) (Schulze et al. 2001), which, together with the above evidence, suggests a crustal source for the phenocrysts. Experimental work conducted in the garnet-stability field has revealed that partial melting of amphibolite would generate silicic melt characterized by low MgO and high SiO₂ (e.g., Skjerlie and Johnston 1996; Rapp et al. 1999), which may well explain the low MgO contents in the garnets and ilmenites from East Kunlun. However, the garnet-bearing tonalite porphyry cannot be entirely ascribed to partial melting of mafic crust, because the rock contains only moderate Sr (<260 ppm), which is significantly lower than the average Sr content (348 ppm) of the lower crust (Rudnick and Gao 2004). Field investigation and geochemical research on the Triassic arc magma in East Kunlun have revealed extensive mixing of crust- and mantle-derived magma (Luo et al. 2002; Liu et al. 2003). In the Nd-Sr isotope correlation diagram (Fig. 10), the garnet-bearing tonalite porphyry plots mainly in the field of Triassic arc magmas, but much closer to the mantle array and therefore distinct from those of the basement of East Kunlun. This may suggest that only a small proportion of crustal component contributed to the genesis of the rock.

Table 6 Whole rock compositions of the garnet-bearing tonalitic porphyry, East Kunlun

Sample	EKL2-01	EKL2-03	EKL2-06	EKL2-08	EKL2-11	EKL2-13	EKL2-16	EKL2-17	EKL2-19	EKL2-21	EKL2-23	EKL2-26	EKL2-28	EKL2-30	EKL2-31	EKL2-33	EKL2-35	EKL2-36	EKL2-37	EKL2-39	EKL2-40
SiO ₂	61.62	61.36	62.18	61.65	61.69	61.64	61.40	62.29	62.09	61.65	61.60	61.48	61.28	60.90	61.07	61.53	61.52	61.94	61.97	62.06	61.83
TiO ₂	0.45	0.45	0.43	0.43	0.44	0.45	0.44	0.43	0.44	0.43	0.43	0.44	0.42	0.41	0.41	0.43	0.43	0.43	0.44	0.44	0.44
Al ₂ O ₃	17.90	17.84	18.13	17.94	17.86	18.02	17.94	18.08	17.98	17.77	17.54	17.50	17.73	17.76	18.06	18.00	18.13	17.95	18.02	17.83	
Fe ₂ O ₃ ^T	5.07	5.05	4.76	4.84	4.80	5.08	4.80	4.83	4.85	4.84	4.83	4.82	4.82	4.85	4.79	4.80	4.81	4.82	4.82	4.82	4.86
MnO	0.08	0.08	0.07	0.08	0.08	0.08	0.07	0.07	0.08	0.08	0.07	0.08	0.08	0.08	0.08	0.08	0.08	0.08	0.08	0.07	0.08
P ₂ O ₅	0.08	0.08	0.09	0.09	0.08	0.09	0.09	0.09	0.09	0.09	0.09	0.09	0.08	0.08	0.08	0.08	0.09	0.09	0.09	0.09	0.09
MgO	1.86	1.86	1.76	1.75	1.72	1.80	1.80	1.77	1.76	1.78	1.77	1.78	1.71	1.75	1.73	1.75	1.74	1.78	1.78	1.78	
CaO	6.45	6.45	6.61	6.59	6.49	6.42	6.39	5.24	5.24	6.32	6.34	6.36	6.35	6.40	6.39	6.44	6.43	6.44	6.52	5.24	6.35
Na ₂ O	3.63	3.76	3.46	3.63	3.30	3.71	3.76	3.60	3.61	3.34	3.29	3.42	3.40	3.27	3.85	3.48	3.41	3.44	3.33	3.60	3.39
K ₂ O	0.87	1.16	1.15	1.09	1.12	1.18	1.19	1.13	1.12	1.05	1.05	1.23	1.25	0.99	0.98	1.10	1.19	1.12	1.12	1.12	1.12
LOI	2.42	2.27	1.82	1.96	2.05	2.13	2.13	2.69	2.74	2.23	2.41	3.01	3.02	3.14	3.06	2.20	2.34	1.96	2.69	2.48	2.48
Total	100.42	100.06	100.46	100.11	99.60	100.54	100.23	100.25	100.03	99.67	99.77	100.06	99.77	99.73	100.51	99.92	99.67	100.43	99.98	99.99	100.24
Li	14.7	14.7	10.5	12.4	15.9	15.1	14.2	22.7	16.2	15.6	17.6	14.7	13.3	12.7	12.8	13.1	14.1	12.1	15.5	18.1	16.0
Be	1.45	1.51	1.52	1.57	1.59	1.62	1.63	1.61	1.71	1.68	1.61	1.76	1.71	1.61	1.62	1.60	1.64	1.57	1.55	1.61	1.58
Sc	7.00	7.37	6.36	6.89	6.57	7.12	6.66	7.59	7.41	6.22	6.97	7.36	6.84	7.44	7.82	6.55	6.62	6.77	7.17	6.57	6.82
V	39.7	41.0	37.3	37.1	37.1	37.2	36.9	36.9	36.1	36.9	38.5	37.4	36.3	35.5	35.3	36.2	36.7	36.2	35.4	35.9	37.6
Cr	15.6	18.0	16.2	16.4	22.4	17.2	15.8	15.1	15.5	16.3	15.7	16.5	17.9	15.7	16.5	21.7	13.6	17.3	15.5	15.8	15.2
Co	9.40	9.70	9.10	9.11	8.84	9.06	8.97	6.80	6.72	8.28	8.16	8.59	8.77	9.73	9.78	7.80	7.82	8.55	6.68	8.22	
Ni	12.6	10.6	11.2	8.5	10.9	8.95	8.28	7.25	8.83	8.45	7.04	8.05	9.55	9.26	8.44	9.76	6.45	8.42	7.83	7.88	6.44
Cu	12.6	12.6	12.8	12.4	12.6	10.8	10.4	10.5	11.9	13.5	13.4	11.9	13.7	10.3	11.2	9.7	9.5	10.0	12.0	10.1	13.0
Zn	77.2	79.9	72.9	73.7	69.4	75.6	71.4	66.4	69.3	73.0	70.3	73.6	74.2	95.3	94.3	73.7	73.0	72.1	70.8	64.3	69.3
Ga	17.1	17.4	17.5	17.8	17.4	17.5	17.0	17.0	16.2	16.6	17.1	16.9	16.9	17.0	16.7	17.3	17.3	16.9	16.6	16.2	16.8
Ge	1.12	1.13	1.11	1.11	1.11	1.10	1.07	1.06	1.05	1.09	1.09	1.18	1.17	1.11	1.17	1.23	1.25	1.21	1.07	1.01	1.11
Rb	35.2	36.1	49.6	49.5	41.9	40.8	40.8	47.6	48.0	43.4	43.3	42.6	43.0	46.0	45.7	46.6	45.4	45.9	40.9	47.7	43.2
Sr	252	259	251	254	249	245	243	208	209	236	236	232	234	240	239	232	230	229	243	208	238
Y	6.66	6.86	6.27	6.27	6.34	6.98	7.04	6.07	5.69	6.72	6.79	6.45	6.42	7.15	7.26	6.96	6.85	6.69	6.24	5.93	6.90
Zr	67.2	72.2	78.3	78.6	72.5	76.9	75.1	68.9	68.6	67.4	75.7	88.4	81.4	82.5	67.0	68.7	77.1	82.0	73.0	67.6	75.6
Nb	3.90	4.01	3.94	3.96	3.97	4.00	3.94	3.85	3.90	3.97	3.96	3.92	3.90	3.86	3.87	3.93	3.85	3.79	3.93	3.88	4.01
Mo	0.76	0.72	0.79	0.70	0.77	0.70	0.64	0.73	0.67	0.48	0.54	0.78	0.89	0.92	0.78	0.64	0.48	0.62	0.65	0.73	0.53
Cd	0.14	0.14	0.17	0.16	0.15	0.21	0.19	0.56	0.19	0.14	0.15	0.18	0.25	0.17	0.19	0.13	0.14	0.18	0.14	0.18	
Sb	0.47	0.48	0.46	0.44	0.54	0.60	0.60	0.89	0.85	0.67	0.69	1.34	1.36	0.93	0.97	0.78	0.83	0.82	0.49	0.84	0.69
Cs	1.21	1.24	1.42	1.40	1.33	1.52	1.52	3.17	314	186	183	259	263	267	341	342	171	170	167	265	182
Ba	247	256	281	282	270	317	314	11.9	11.5	10.8	11.4	11.7	11.5	11.6	11.4	36.1	33.4	34.5	11.2	11.3	11.7
La	11.3	13.0	11.2	11.5	11.1	11.8	11.9	23.1	22.7	21.1	22.1	22.5	22.3	22.1	22.1	66.8	61.1	63.2	22.1	21.9	23.0
Ce	22.5	24.9	21.9	22.6	21.7	23.0	23.1	22.7	21.1	22.4	22.1	22.5	22.3	22.1	22.1	22.1	22.1	22.1	22.1	22.1	22.1
Pr	2.70	3.02	2.67	2.70	2.64	2.74	2.84	2.74	2.59	2.72	2.79	2.65	2.74	2.67	2.66	2.66	2.67	2.66	2.65	2.65	2.84
Nd	10.7	11.5	10.6	10.7	10.4	10.8	10.7	10.5	9.8	10.6	10.9	10.6	10.6	10.4	10.3	25.1	23.0	23.7	10.3	10.3	11.0
Sm	2.24	2.36	2.23	2.24	2.19	2.18	2.29	2.14	2.04	2.23	2.25	2.17	2.16	2.13	2.13	3.62	3.44	3.48	2.17	2.06	2.35
Eu	0.73	0.75	0.76	0.73	0.74	0.72	0.71	0.68	0.74	0.77	0.73	0.74	0.75	0.74	0.75	0.90	0.89	0.87	0.74	0.69	0.77
Gd	1.84	1.94	1.81	1.80	1.86	1.87	1.72	1.63	1.87	1.83	1.83	1.81	1.82	1.81	1.81	2.86	2.71	2.73	1.77	1.67	1.87
Tb	0.26	0.27	0.26	0.25	0.26	0.26	0.25	0.24	0.24	0.26	0.26	0.25	0.26	0.26	0.27	0.32	0.31	0.31	0.26	0.23	0.27
Dy	1.34	1.35	1.30	1.28	1.31	1.39	1.38	1.24	1.20	1.36	1.33	1.30	1.31	1.42	1.38	1.49	1.45	1.40	1.26	1.21	1.39

Table 6 continued

Sample	EKL2-01	EKL2-03	EKL2-06	EKL2-08	EKL2-11	EKL2-13	EKL2-16	EKL2-17	EKL2-19	EKL2-21	EKL2-23	EKL2-26	EKL2-28	EKL2-30	EKL2-31	EKL2-33	EKL2-35	EKL2-36	EKL2-37	EKL2-39	EKL2-40	
Ho	0.25	0.26	0.24	0.24	0.24	0.27	0.23	0.22	0.26	0.25	0.24	0.26	0.25	0.27	0.27	0.26	0.24	0.26	0.22	0.24	0.26	
Er	0.69	0.72	0.66	0.66	0.67	0.78	0.76	0.68	0.64	0.72	0.71	0.68	0.67	0.79	0.78	0.78	0.74	0.76	0.65	0.66	0.66	
Tm	0.10	0.10	0.09	0.09	0.09	0.11	0.11	0.09	0.08	0.10	0.10	0.09	0.09	0.11	0.11	0.10	0.10	0.10	0.09	0.09	0.11	
Yb	0.61	0.63	0.58	0.56	0.58	0.70	0.71	0.59	0.55	0.64	0.63	0.60	0.59	0.73	0.71	0.66	0.64	0.62	0.59	0.56	0.64	
Lu	0.09	0.09	0.08	0.08	0.09	0.10	0.10	0.09	0.08	0.09	0.09	0.08	0.09	0.10	0.11	0.10	0.09	0.09	0.08	0.08	0.09	
Hf	2.03	2.18	2.32	2.37	2.17	2.31	2.24	2.06	2.07	2.05	2.22	2.58	2.40	2.35	1.97	2.09	2.26	2.34	2.16	1.96	2.19	
Pb	9.52	9.48	11.01	10.89	11.27	9.56	9.59	10.11	10.85	10.17	11.30	9.93	11.99	10.44	10.80	9.80	9.97	10.12	11.14	10.10	10.18	
Ta	0.33	0.32	0.31	0.31	0.32	0.30	0.30	0.29	0.30	0.30	0.30	0.30	0.29	0.29	0.29	0.29	0.29	0.28	0.30	0.28	0.30	
W	0.44	0.42	0.34	0.32	0.34	0.33	0.29	0.56	0.49	0.29	0.32	0.40	0.42	0.36	0.36	0.36	0.36	0.30	0.25	0.27	0.31	
Tl	0.24	0.25	0.32	0.31	0.26	0.31	0.29	0.37	0.38	0.25	0.26	0.30	0.31	0.33	0.32	0.25	0.25	0.24	0.27	0.27	0.27	
Bi	0.09	0.09	0.05	0.05	0.08	0.06	0.06	0.12	0.12	0.14	0.15	0.12	0.13	0.05	0.05	0.05	0.05	0.16	0.16	0.17	0.07	
Th	3.65	4.19	3.71	3.83	3.62	3.91	3.94	3.88	3.66	3.66	3.81	3.81	3.75	3.67	3.55	12.36	13.05	3.65	3.72	3.73	3.73	
U	1.29	1.33	1.40	1.40	1.36	1.37	1.34	1.28	1.23	1.34	1.38	1.48	1.47	1.35	1.39	1.62	1.56	1.58	1.33	1.25	1.38	
ACNR ^a	0.93	0.92	0.93	0.91	0.94	0.92	0.91	1.04	1.04	0.95	0.95	0.93	0.93	0.93	0.89	0.95	0.95	0.96	0.94	1.04	0.94	
Mg# ^b	48	48	48	48	47	47	48	48	48	48	48	48	47	47	48	48	48	48	48	48	48	
REE	55.3	61.0	54.4	55.5	53.8	56.7	57.0	55.3	51.7	55.1	56.1	55.0	55.3	55.1	54.8	146.3	134.9	139.0	54.1	53.6	57.1	
(La/Yb) _{Ch} ^b	12.6	13.9	13.0	13.8	13.0	11.4	11.3	13.1	13.4	12.1	12.6	12.8	13.1	10.7	10.8	37.2	35.3	37.9	12.9	13.6	12.3	
(Gd/Yb) _{Ch} ^b	3.69	3.73	3.78	3.88	3.79	3.23	3.20	3.51	3.62	3.57	3.52	3.68	3.70	3.01	3.08	5.30	5.14	5.39	3.66	3.59	3.52	
Eu*	1.09	1.07	1.16	1.15	1.13	1.13	1.06	1.13	1.14	1.11	1.16	1.12	1.12	1.14	1.17	0.85	0.89	0.86	1.15	1.14	1.12	
Ce*	0.95	0.93	0.94	0.95	0.94	0.95	0.93	0.95	0.93	0.93	0.92	0.95	0.93	0.93	0.94	0.96	0.96	0.96	0.95	0.94	0.94	
Zr/Sn	30	31	35	35	33	35	33	32	34	30	34	41	36	38	38	32	19	22	24	34	33	32
Zr/Yb	110	114	134	140	126	110	106	116	126	106	120	146	137	113	94	105	121	133	124	120	117	
Nb/Yb	6.42	6.36	6.76	7.05	6.89	5.71	5.55	6.47	7.14	6.23	6.27	6.49	6.57	5.26	5.42	5.99	6.02	6.15	6.67	6.90	6.23	
Th/Nb	0.93	1.04	0.94	0.97	0.91	0.98	1.00	1.01	0.94	0.92	0.96	0.97	0.98	0.97	0.95	3.45	3.21	3.45	0.93	0.96	0.93	
Zr/Nb	17	18	20	20	18	19	19	18	18	17	19	23	21	21	17	17	20	22	19	17	19	
Th/La	0.32	0.32	0.33	0.33	0.33	0.33	0.33	0.34	0.34	0.32	0.33	0.32	0.32	0.32	0.32	0.38	0.37	0.38	0.32	0.33	0.32	
Sr/Y	37.9	37.7	40.1	40.5	39.3	35.0	34.5	34.3	36.7	35.1	34.8	36.0	36.4	33.6	33.0	33.3	33.5	34.2	38.9	35.1	34.4	
Ce/Pb	2.4	2.6	2.0	2.1	1.9	2.4	2.2	2.4	2.2	1.9	2.2	2.0	2.2	1.9	2.1	2.0	6.8	6.1	6.3	2.0	2.2	
^e Nd ^c	-1.8	-2.0	-2.1	-2.1	-1.9	-2.3	-1.9	-2.3	-1.9	-2.3	-1.8	-1.8	-1.4	-1.4	-1.4	-1.4	-2.0	-2.0	-2.0	-2.0	-2.0	
Initial Sr ^d	0.7067	0.7066	0.7067	0.7066	0.7066	0.7066	0.7066	0.7066	0.7066	0.7066	0.7066	0.7066	0.7066	0.7066	0.7066	0.7066	0.7066	0.7066	0.7066	0.7066		

^a Aluminum saturation index = molar Al₂O₃/[K₂O + Na₂O + CaO]^b Chondrite data from Taylor and McLennan 1985^c λ_{Sm} = 6.54 × 10⁻¹² year⁻¹^d λ_{Rb} = 1.42 × 10⁻¹¹ year⁻¹

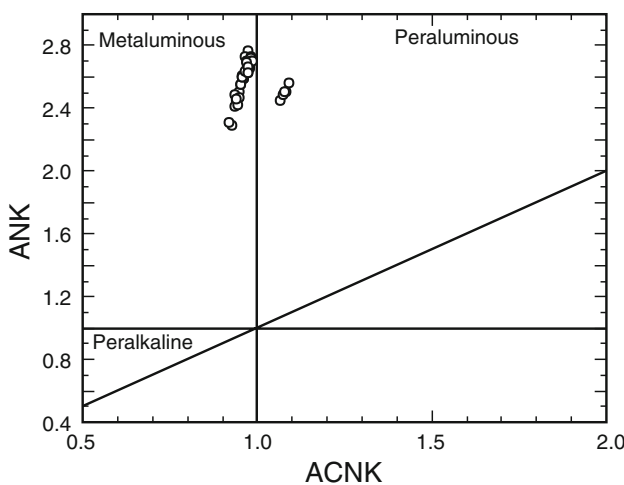


Fig. 7 ANK versus ACNK diagram for the granitoids from East Kunlun (after Maniar and Piccoli 1989)

Plagioclase phenocrysts record the compositional variation of the magma during a later stage of its crystallization. The reversed zoning in plagioclase (Table 3) is commonly considered to reflect magma mixing with a more primitive source (Hibbard 1995; Kawabata and Shuto 2005). Because dehydration melting of lower crust requires relatively high temperature ($>850^{\circ}\text{C}$) (e.g., Rushmer 1991; Sen and Dunn 1994; Skjerlie and Johnston 1996), a mantle-derived magma must have been involved to fuse the crustal material. The high Al_2O_3 and mostly positive Eu anomalies of the tonalite porphyry suggest retarded crystallization of plagioclase, which, together with the abundant hornblende in the rock, indicates an H_2O -rich magma (Müntener et al. 2001; Grove et al. 2002). Due to the scarcity of water in the lower crust, partial melting of lower crust cannot generate

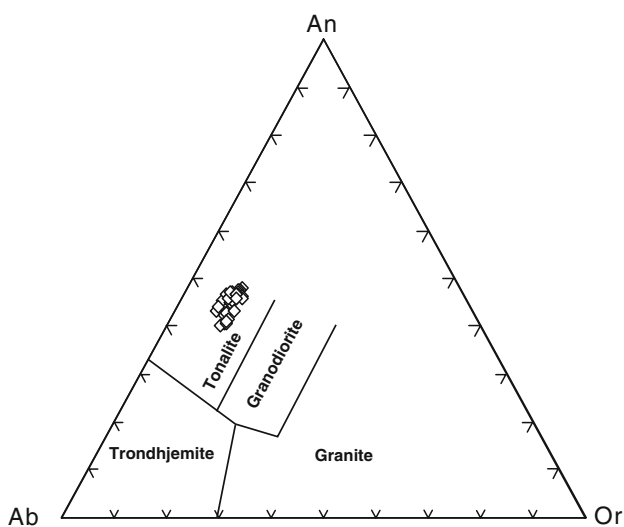


Fig. 8 An-Ab-Or CIPW-normative ternary diagram for the granitoids from East Kunlun (after Barker 1979)

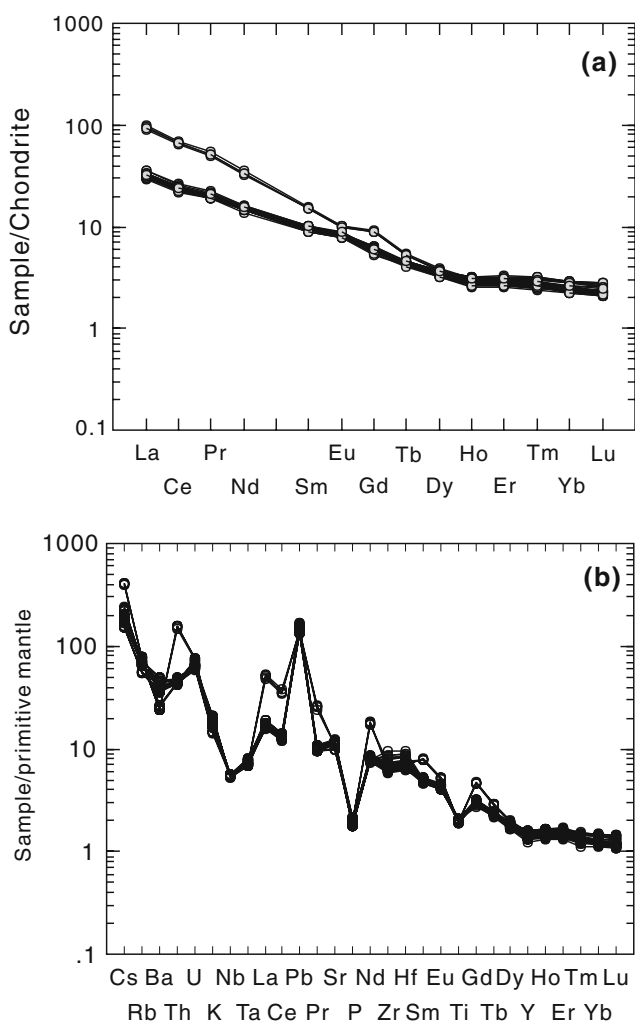


Fig. 9 Trace element characteristics of the garnet-bearing tonalite porphyry **(a)** Chondrite-normalized rare earth element patterns for representative samples of the tonalite porphyry, East Kunlun (chondrite values from Taylor and McLennan 1985). **b** Primitive mantle-normalized trace element spider diagrams for representative samples of the tonalite porphyry, East Kunlun (Primitive mantle data from Sun and McDonough 1989)

an H_2O -rich melt (Patiño Douce 1999), therefore the high H_2O contents in the garnet-bearing tonalitic porphyry most likely came from mantle-derived magma. In the Triassic, the Paleo-Tethys was being consumed along the south margin of the Kunlun arc (Yin and Harrison 2000), which resulted in widespread arc magmatism in East Kunlun. It is therefore likely that mantle-derived arc magma was underplated along the crust-mantle zone and mixed with a felsic crustal melt, a scenario consistent with experimental work conducted by McCarthy and Patiño Douce (1997).

In terms of tectonic setting, Paleo-Tethys was still being consumed along the Kunlun in the late Triassic (Sengör 1987; Yin and Harrison 2000), and Triassic limestone within flysch sediments in the Kunlun range suggest a marine-phase sedimentary environment that probably

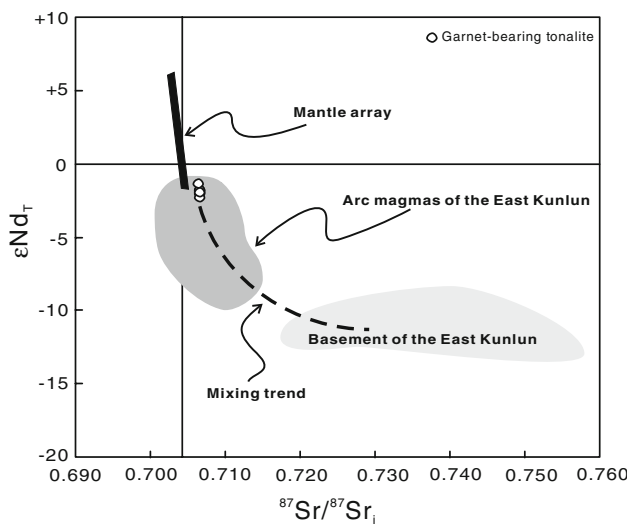


Fig. 10 Correlation diagram between $^{87}\text{Sr}/^{86}\text{Sr}_i$ and ϵNd_T for garnet-bearing tonalitic porphyry. (Data for the basement of East Kunlun from Yu et al. 2005; data for the arc magmas of East Kunlun from Chen et al. 2005 and Liu et al. 2003)

reflected a normal crustal thickness (~ 35 km) for the East Kunlun at this time. Therefore, although there is no direct evidence of restite or xenoliths indicating generation at the crust-mantle boundary, the high pressure of the garnet phenocrysts may indicate that they were formed at, or just above, the crust-mantle transition zone. The garnet-bearing tonalite porphyry from East Kunlun therefore provides a paradigm of MASH zone magmatic processes.

Implications for genesis of adakitic rocks

Adakites are sodic rocks characterized by low HREE but elevated Sr and Al_2O_3 contents and high Sr/Y and La/Yb ratios, which are ascribed to hydrous partial melting of a subducted oceanic slab or over-thickened lower crust in the garnet stability field (Defant and Drummond 1990; Atherton and Petford 1993; Martin et al. 2005). Because of the broad similarity to Archean tonalite–trondhjemite–granodiorite gneisses (TTG) and their potential role in metallogenesis (Martin 1999; Smithies 2000; Condie 2005; Richards and Kerrich 2007), adakitic rocks have received much attention. Although the petrogenetic regime has been supported by much experimental work (e.g., Rapp et al. 1991; Rushmer 1991; Sen and Dunn 1994), most thermal models require subduction of young, and therefore warm, oceanic lithosphere to reach the temperature of the wet basaltic solidus at depths of 90–120 km (e.g., Peacock et al. 1994). However, such a prediction is contrary to many modern cases where adakites occur in association with old, and thus cold, subducting slabs (Macpherson et al. 2006). To deal with such a paradox, some workers have proposed that fractional crystallization of H_2O -rich

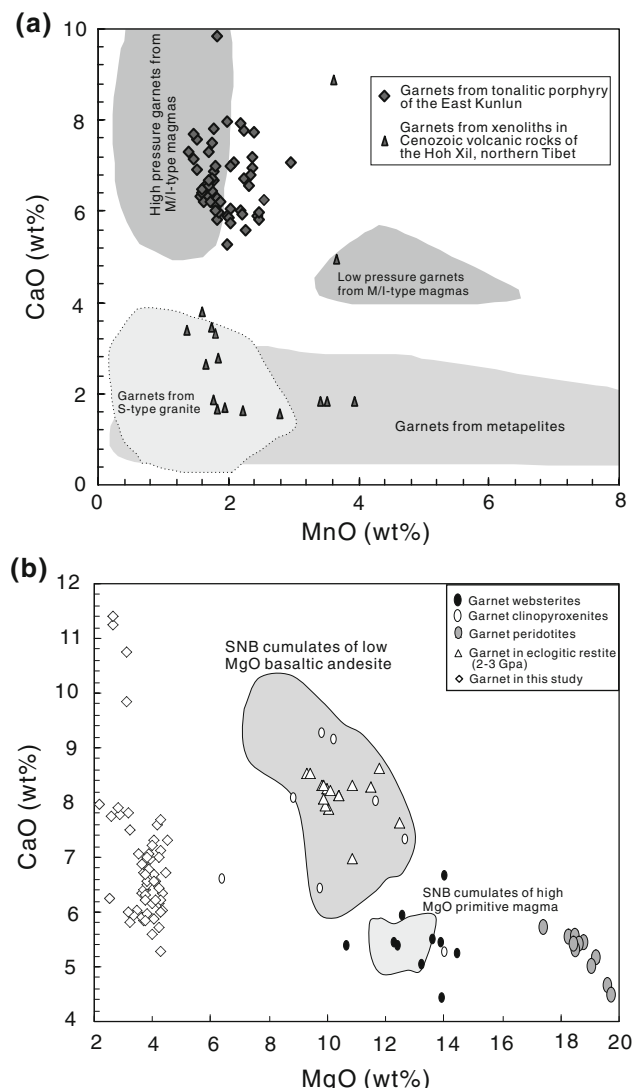


Fig. 11 Garnet comparisons in this study compared to other settings. **a** CaO versus MnO correlation diagram (after Harangi et al. 2001) Data for Cenozoic volcanic rocks of the Hoh Xil, northern Tibet from Deng (1998). **b** CaO versus MgO correlation diagram (after Lee et al. 2006) SNB: Sierra Nevada Batholith; data for garnet in eclogite restite from Pertermann and Hirschmann (2003)

arc magmas under high pressure conditions would give rise to adakitic signatures in arc magmas (e.g., Castillo et al. 1999; Kleinhanns et al. 2003; Macpherson et al. 2006; Eiler et al. 2007; Richards and Kerrich 2007; Roderíguez et al. 2007). However, both adakitic and non-adakitic rocks may come from the mantle and experience high pressure fractionation in the MASH zone, therefore there must be other key factors affecting the composition of arc magmas that prevent some from becoming adakitic rocks.

It is proposed that the garnet-bearing tonalite porphyry from East Kunlun experienced strong fractional crystallization and magma mixing in the garnet stability field, therefore providing an opportunity to test the various

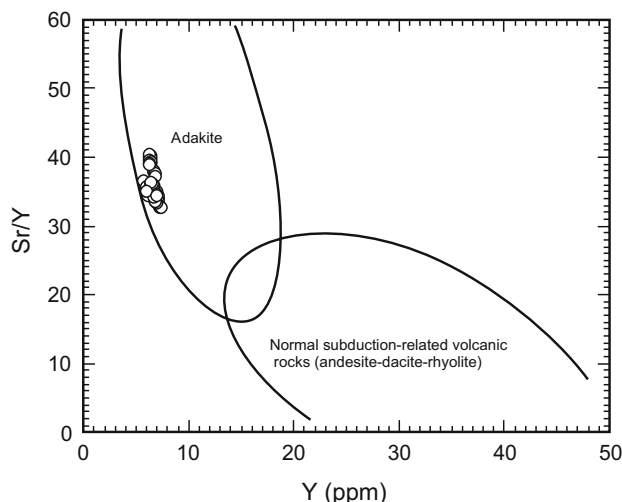


Fig. 12 Sr/Y versus Y correlation diagram for discrimination of adakites (after Defant and Drummond 1990)

hypotheses. It contains relatively high Al_2O_3 (>17 wt%), mostly positive Eu anomalies ($\text{Eu}/\text{Eu}^* > 1.1$) and high Zr/Sr ratios (>30). The low HREE ($\text{Yb} < 0.8 \text{ ppm}$) and high Sr/Y (>33) ratios are significantly differ from those of normal island arc magmas. In the Y versus Sr/Y correlation diagram, all tonalite rock samples plot in the adakite field (Fig. 12). These features suggest that fractional crystallization of H_2O -rich arc magma in the garnet stability field can effectively scavenge HREE and generate Al-rich melt. However, there are some differences between the tonalite porphyry and adakitic rocks. The porphyry has moderate Sr (<260 ppm) and La/Yb ratios (16–21), which are lower than those of adakite (Sr > 400 ppm; La/Yb ≥ 20) and TTG (Sr > 500 ppm; La/Yb generally >30) (Barker 1979; Richards and Kerrich 2007). Because plagioclase was suppressed by the high water content in the magma, removal of Sr by fractionation of plagioclase can be excluded. Instead, crystallization of apatite at an early stage of magmatic evolution may be responsible for the relatively low Sr contents and La/Yb ratios in the residual melt. Apatite commonly occurs in mantle and crustal environments and possesses high partition coefficients for both Sr and LREE (Chazot et al. 1996; Bea and Montero 1999). For example, apatite may concentrate LREE up to 200 times compared to clinopyroxene and, although slightly lower than that of plagioclase (up to 15.8) (Ren et al. 2003), its partition coefficient for Sr ($D_{\text{Sr}} = 5.1\text{--}8.2$) is still high enough to affect magma composition (Plá Cid et al. 2007; Prowatke and Klemme 2006). Petrographic observation of the tonalite porphyry reveals that apatite is mainly enclosed in the garnet phenocrysts which, along with the depletion in P in the spider diagram (Fig. 9b), implies removal of apatite as an early phase during evolution of the magma in the MASH zone. Because plagioclase was suppressed by a high

water content in the early stage of magmatic evolution, Sr concentration in the residual melt would be mainly controlled by apatite. Similarly, moderate Sr contents (<400 ppm) and apatite inclusions in garnet phenocrysts appear to be common features of garnet-bearing intermediate rocks worldwide (e.g., Day et al. 1992; Harangi et al. 2001; Bach et al. 2003; Kawabata and Shuto 2005), implying that apatite has played a crucial role in buffering the Sr level in the magmas. It is therefore suggested that mantle-derived arc magmas cannot evolve into adakites when extensive crystallization of apatite has already occurred in the MASH zone.

Conclusions

The garnet-bearing tonalitic porphyry from the East Kunlun formed in the late Triassic ($213 \pm 3 \text{ Ma}$), related to consumption of the Paleo-Tethys ocean. It contains phenocrysts of garnet, hornblende, plagioclase and quartz that crystallized in an H_2O -rich magma. The relatively low MgO contents of garnet and ilmenite and high $\delta^{18}\text{O}$ value of garnet separates suggest these early phases were formed in a felsic melt. Pressure estimates for hornblende enclosing garnet provide a minimum constraint on the formation depth of the garnet phenocrysts (8–10 kb), suggesting they were produced at or just above the crust-mantle transition zone (MASH zone). Nd–Sr isotope compositions indicate involvement of both crust- and mantle-derived magma and reversed compositional zoning of plagioclase implies magma mixing. Although the garnet-bearing tonalitic porphyry resembles an adakitic rock in many respects, the relatively low Sr content and La/Yb ratio makes it distinct from ‘true’ adakites. It is proposed that early crystallization of apatite may effectively remove Sr and LREE from the magma, thus providing a mechanism whereby some arc magmas do not evolve into adakite.

Acknowledgments We thank Qian Mao, Yuguang Ma and Ms. Ying Liu for their help with the analytical work. The authors benefited from discussions with Drs Guochun Zhao, Hongfu Zhang, Nengsong Chen, Chunming Wu and Petra Bach. We also appreciate the constructive and encouraging comments of reviewers Ali Polat and Fu-yuan Wu, which helped us to improve and clarify the manuscript. This work was supported by research grants from the National Basic Research Program of China (973 Program) 2007CB411308, NSFC Projects 40421303, 40572043, 40725009 and Hong Kong RGC (HKU 7040/04).

References

- Ague JJ (1997) Thermodynamic calculation of emplacement pressures for batholithic rocks, California: implications for the aluminum-in-hornblende barometer. *Geology* 25:563–566. doi:10.1130/0091-7613(1997)025<0563:TCOEPF>2.3.CO;2

- Anderson JL (1996) Status of thermobarometry in granitic batholith. *Trans R Soc Edinb Earth Sci* 87:125–138
- Anderson DL (2006) Speculations on the nature and cause of mantle heterogeneity. *Tectonophysics* 416:7–22. doi:[10.1016/j.tecto.2005.07.011](https://doi.org/10.1016/j.tecto.2005.07.011)
- Annen C, Blundy JD, Sparks RSJ (2006) The genesis of intermediate and silicic magmas in deep crustal hot zones. *J Petrol* 47:505–539. doi:[10.1093/petrology/egi084](https://doi.org/10.1093/petrology/egi084)
- Atherton MP, Petford N (1993) Generation of sodium-rich magmas from newly underplated basaltic crust. *Nature* 362:144–146. doi:[10.1038/362144a0](https://doi.org/10.1038/362144a0)
- Bach P, Malpas J, Smith IEM (2003) A petrogenetic link between high-MgO and garnet-bearing andesites—a Setouchi analogue from the Eastern volcanic belt in Northland, New Zealand? *Geochim Cosmochim Acta* 67:A30–A30. doi:[10.1016/S0016-7037\(03\)00304-1](https://doi.org/10.1016/S0016-7037(03)00304-1) Suppl
- Bandrés A, Egúmez L, Pin C, Paquette JL, Ordóñez B, Le Fèvre B et al (2004) The northern Ossa-Morena Cadomian batholith (Iberian Massif): magmatic arc origin and early evolution. *Int J Earth Sci* 93:860–885. doi:[10.1007/s00531-004-0423-6](https://doi.org/10.1007/s00531-004-0423-6)
- Barker F (1979) Trondhjemite: definition, environment and hypotheses of origin. In: Barker F (ed) *Trondhjemite*. Dacite and related rocks. Elsevier, Amsterdam, pp 1–12
- Bea F, Montero P (1999) Behavior of accessory phases and redistribution of Zr, REE, Y, Th, and U during metamorphism and partial melting of metapelites in the lower crust: An example from the Kinzigite Formation of Ivrea-Verbano, NW Italy. *Geochim Cosmochim Acta* 63:1133–1153. doi:[10.1016/S0016-7037\(98\)00292-0](https://doi.org/10.1016/S0016-7037(98)00292-0)
- Behn MD, Kelemen PB (2006) Stability of arc lower crust: Insights from the Talkeetna arc section, south central Alaska, and the seismic structure of modern arcs. *J Geophys Res Solid Earth* 111:B11207. doi:[10.1029/2006JB004327](https://doi.org/10.1029/2006JB004327)
- Berger J, Féminias O, Coussaert N, Mercier JCC, Demaiffe D (2007) Cumulating processes at the crust-mantle transition zone inferred from Permian mafic-ultramafic xenoliths (Puy Beaunit, France). *Contrib Mineral Petrol* 153:557–575. doi:[10.1007/s00410-006-0162-8](https://doi.org/10.1007/s00410-006-0162-8)
- Bian QT, Li DH, Pospelov I, Yin LM, Li HS, Zhao DS et al (2004) Age, geochemistry and tectonic setting of Buqingshan ophiolites, North Qinghai-Tibet Plateau, China. *J Asian Earth Sci* 23:577–596. doi:[10.1016/j.jseas.2003.09.003](https://doi.org/10.1016/j.jseas.2003.09.003)
- Birch WD, Gleadow JW (1974) The genesis of garnet and Cordierite in acid volcanic rocks: evidence from the Cerberean Cauldron, Central Victoria, Australia. *Contrib Mineral Petrol* 45:1–13. doi:[10.1007/BF00371133](https://doi.org/10.1007/BF00371133)
- Bryant JA, Yogodzinski GM, Churikova TG (2007) Melt-mantle interactions beneath the Kamchatka arc: evidence from ultramafic xenoliths from Shiveluch volcano. *Geochim Geophys Geosyst* 8:Q04007. doi:[10.1029/2006GC001443](https://doi.org/10.1029/2006GC001443)
- Castillo PR, Janney PE, Solidum RU (1999) Petrology and geochemistry of Camiguin Island, southern Philippines: insights to the source of adakites and other lavas in a complex arc setting. *Contrib Mineral Petrol* 134:33–51. doi:[10.1007/s004100050467](https://doi.org/10.1007/s004100050467)
- Chang C, Chen N, Coward MP, Deng W, Dewey JF, Gansser A et al (1986) Preliminary conclusions of the Royal society and Academia Sinica 1985 geotraverse of Tibet. *Nature* 323:501–507. doi:[10.1038/323501a0](https://doi.org/10.1038/323501a0)
- Chazot G, Menzies MA, Harte B (1996) Determination of partition coefficients between apatite, clinopyroxene, amphibole, and melt in natural spinel lherzolites from Yemen: implications for wet melting of the lithospheric mantle. *Geochim Cosmochim Acta* 60:423–437. doi:[10.1016/0016-7037\(95\)00412-2](https://doi.org/10.1016/0016-7037(95)00412-2)
- Chen NS, Wang XY, Zhang HF, Sun M, Li XY, Chen Q (2005) Geochemistry and Nd-Sr-Pb isotopic compositions of granitoids from Qaidam and Oulongbuluke micro-blocks, NW China: constraints on basement nature and tectonic affinity. *Earth Sci J China Univ Geosci* 32:7–21
- Chen NS, Li XY, Zhang KX, Wang GC, Zhu YH, Hou GJ et al (2006) Lithological characteristics of the Baishaha formation to the South of Xiangride Town, Eastern Kunlun Mountains and its age constrained from Zircon Pb-Pb dating. *Geol Sci Technol Inf* 25:1–7
- CIGMR (Chengdu Institute of Geology and Mineral Resources) (1988) Notes for the geological map of Tibet-Qinghai Plateau and adjacent areas (1:1,500,000). Geological Publication House, Beijing, pp 1–60
- Compston W, Williams IS, Meyer C (1984) U-Pb geochronology of zircons from Lunar breccia 73217 using a sensitive high massresolution ion microprobe. *J Geophys Res* 89B:525–534. doi:[10.1029/JB089iS02p0B525](https://doi.org/10.1029/JB089iS02p0B525)
- Condie KC (2005) TTGs and adakites: are they both slab melts? *Lithos* 80:33–44. doi:[10.1016/j.lithos.2003.11.001](https://doi.org/10.1016/j.lithos.2003.11.001)
- Conrad WK, Nicholls LA, Wall VJ (1988) Water-saturated and unsaturated melting of metaluminous and peraluminous crustal compositions at 10 kb: evidence for the origin of silicic magmas in the Taupo Volcanic Zone, New Zealand and other occurrence. *J Petrol* 29:765–803
- Cowgill E, Yin A, Harrison TM, Wang X-F (2003) Reconstruction of the Altyn Tagh fault based on U-Pb geochronology: role of back thrusts, mantle sutures, and heterogeneous crustal strength in forming the Tibetan Plateau. *J Geophys Res* 108:2346. doi:[10.1029/2002JB002080](https://doi.org/10.1029/2002JB002080)
- Day RA, Green TH, Smith IEM (1992) The Origin and Significance of garnet phenocrysts and garnet-bearing xenoliths in Miocene calc-alkaline volcanics from Northland, New Zealand. *J Petrol* 33:125–161
- Defant MJ, Drummond MS (1990) Derivation of some modern arc magmas by melting of young subducted lithosphere. *Nature* 347:662–665. doi:[10.1038/347662a0](https://doi.org/10.1038/347662a0)
- Deng WM (1998) Cenozoic intraplate volcanic rocks in the northern Qinghai-Xizang Plateau (in Chinese with English abstract). Geological Publishing House, Beijing, pp 1–180
- Dewey JF, Shackleton RS, Chang CF, Sun YY (1988) The tectonic evolution of the Tibetan Plateau. *Philos Trans R Soc Lond* 327:379–413. doi:[10.1098/rsta.1988.0135](https://doi.org/10.1098/rsta.1988.0135)
- Dufek J, Bergantz GW (2005) Lower crustal magma genesis and preservation: a stochastic framework for the evaluation of basalt-crust interaction. *J Petrol* 46:2167–2195. doi:[10.1093/petrology/egi049](https://doi.org/10.1093/petrology/egi049)
- Eiler JM, Schiano P, Valley JW, Kita NT, Stolper EM (2007) Oxygen-isotope and trace element constraints on the origins of silica-rich melts in the subarc mantle. *Geochem Geophys Geosyst* 8:Q09012–00. doi:[10.1029/2006GC001503](https://doi.org/10.1029/2006GC001503)
- Foley S, Tiepolo M, Vannucci R (2002) Growth of early continental crust controlled by melting of amphibolite in subduction zones. *Nature* 417:837–840. doi:[10.1038/nature00799](https://doi.org/10.1038/nature00799)
- Franchini M, López-Escobar L, Schalamuk IBA, Meinert L (2003) Magmatic characteristics of the Paleocene Cerro Nevazón region and other Late Cretaceous to Early Tertiary calc-alkaline subvolcanic to plutonic units in the Neuquén Andes, Argentina. *J S Am Earth Sci* 16:399–421. doi:[10.1016/S0895-9811\(03\)00103-2](https://doi.org/10.1016/S0895-9811(03)00103-2)
- Garrido CJ, Bodinier J-L, Burg J-P, Zeilinger G, Hussain SS, Dawood H et al (2006) Petrogenesis of mafic garnet granulite in the lower crust of the Kohistan Paleo-arc complex (northern Pakistan): implications for Intra-crustal differentiation of island arcs and generation of continental crust. *J Petrol* 47:1873–1914. doi:[10.1093/petrology/egl030](https://doi.org/10.1093/petrology/egl030)
- Gehrels GE, Yin A, Wang X (2003b) Magmatic history of the northeastern Tibetan Plateau. *J Geophys Res* 108(B9):2423. doi:[10.1029/2002JB001876](https://doi.org/10.1029/2002JB001876)

- Gehrels GE, Yin A, Wang X-F (2003a) Detrital zircon geochronology of the northeastern Tibetan plateau. *Geol Soc Am Bull* 115: 881–896. doi:10.1130/0016-7606(2003)115<0881:DGOTNT>2.0.CO;2
- Gilbert JS, Rogers NW (1989) The significance of garnet in the Permo-carboniferous volcanic rocks of the Pyrenees. *J Geol Soc London* 146:477–490. doi:10.1144/gsjgs.146.3.0477
- Green TH (1977) Garnet in Silicic liquids and its possible use as a P-T indicator. *Contrib Mineral Petrol* 65:59–67. doi:10.1007/BF00373571
- Green TH (1992) Experimental phase equilibrium studies of garnet-bearing I-type volcanics and high-level intrusives from Northland, New Zealand. *Trans R Soc Edinb Earth Sci* 83:429–438
- Greene AR, DeBari SM, Kelemen PB, Blusztajn J, Clift PD (2006) A detailed geochemical study of island arc crust: the Talkeetna arc section, South-Central Alaska. *J Petrol* 47:1051–1093. doi:10.1093/petrology/egl002
- Grove TL, Parman SW, Bowring SA, Price RC, Baker MB (2002) The role of H₂O-rich fluid component in the generation of primitive basaltic andesites and andesites from the Mt Shasta region, N California. *Contrib Mineral Petrol* 251:229–250
- Harangi SZ, Downes H, Kósa L, Szabó CS, Thirlwall MF, Mason PRD et al (2001) Almandine garnet in calc-alkaline volcanic rocks of the Northern Pannonian Basin (Eastern-Central Europe): geochemistry, petrogenesis and geodynamic implications. *J Petrol* 42:1813–1843. doi:10.1093/petrology/42.10.1813
- Hawthorne FC (1981) The crystal chemistry of the amphiboles. In: Veblen DR (ed) *Amphiboles and other hydrous pyroboles—mineralogy*. Mineralogical Society of America, Reviews in Mineralogy 9 m, pp 1–140
- Hermann J, Müntener O, Trommsdorff V, Hansmann W (1997) Fossil crust-to-mantle transition, Val Malenco (Italian Alps). *J Geophys Res* 102:20,123–20,132. doi:10.1029/97JB01510
- Hibbard MJ (1995) Petrography to petrogenesis. Prentice Hall, Englewood Cliffs, pp 1–586
- Hildreth W, Moorbath S (1988) Crustal contributions to arc magmatism in the Andes of central Chile. *Contrib Mineral Petrol* 98:455–489. doi:10.1007/BF00372365
- Holdaway MJ, Mukhopadhyay B, Dyar MD, Guidotti CV, Dutrow BL (1997) Garnet-biotite geothermometry revised: new Margules parameters and a natural specimen data set from Maine. *Am Mineral* 82:582–595
- Holland T, Blundy J (1994) Nonideal interactions in clastic amphiboles and their bearing on amphibole-plagioclase thermometry. *Contrib Mineral Petrol* 116:433–447. doi:10.1007/BF00310910
- Jiang CF (1992) Opening-closing evolution of the Kunlun Mountains. In: Jiang C, Yang J, Feng B, Zhu Z, Zhao M, Chai Y, Shi X, Wang H, Hu J (eds) *Opening closing tectonics of Kunlun Shan. Geological Memoirs, Series 5, Number 12*, pp 205–217. Geological Publishing House, Beijing, China
- Kawabata H, Shuto K (2005) Magma mixing recorded in intermediate rocks associated with high-Mg andesites from the Setouchi volcanic belt, Japan: implications for Archean TTG formation. *J Volcanol Geotherm Res* 140:241–271. doi:10.1016/j.jvolgeores.2004.08.013
- Kawabata H, Takafuji N (2005) Origin of garnet crystals in calc-alkaline volcanic rocks from the Setouchi volcanic belt, Japan. *Mineral Mag* 69:951–971. doi:10.1180/0026461056960301
- Kleinhanus IC, Kramers JD, Kamber BS (2003) Importance of water for Archean granitoid petrology: a comparative study of TTG and potassic granitoids from Barberton Mountain Land, South Africa. *Contrib Mineral Petrol* 145:377–389. doi:10.1007/s00410-003-0459-9
- Lan CL, Wu J, Li JL, Yu LJ, Li HS, Wang YT (2000) Discovery of early Carboniferous radiolarians in Muztag ophiolitic mélange, East Kunlun, Xinjiang (in Chinese with English abstract). *Chin J Geol* 37:104–106 in Chinese with English abstract
- Lee CTA, Cheng X, Horodyskyj U (2006) The development and refinement of continental arcs by primary basaltic magmatism, garnet pyroxenite accumulation, basaltic recharge and delamination: insights from the Sierra Nevada California. *Contrib Mineral Petrol* 151:222–242. doi:10.1007/s00410-005-0056-1
- Li XH (1997) Geochemistry of the Longsheng Ophiolite from the southern margin of Yangtze Craton, SE China. *Geochem J* 31:323–337
- Li YJ, Jia CZ, Hao J, Wang ZM, Zheng DM, Peng GX (2000) Radiolarian fauna found from Tieshdas Group in East Kunlun. *Chin Sci Bull* 45:943–946. doi:10.1007/BF02887089
- Liu CD, Mo XX, Luo ZH, Yu XH, Chen HW, Li SW et al (2003) Pb–Sr–Nd–O isotope characteristics of granitoids in East Kunlun Orogenic Belt (in Chinese with English abstract). *Acta Geosci Sin* 24:584–588
- Liu JB, Ye K (2004) Transformation of garnet epidote amphibolite to eclogite, western Dabie Mountains, China. *J Metamorph Geol* 22:383–394. doi:10.1111/j.1525-1314.2004.00520.x
- Liu YJ, Genser J, Neubauer F, Jin W, Ge XH, Handler R et al (2005) Ar-40/Ar-39 mineral ages from basement rocks in the Eastern Kunlun Mountains, NW China, and their tectonic implications. *Tectonophysics* 398:199–224. doi:10.1016/j.tecto.2005.02.007
- Ludwig KR (2001) Users Manual for a geochronological toolkit for Microsoft Excel, Berkeley Geochronology Center. Spec Publ 1a:59
- Luo ZH, Deng JF, Cao YQ, Guo ZF, Mo XX (1999) On Late Paleozoic-Early Mesozoic volcanism and regional tectonic Evolution of Eastern Kunlun, Qinghai Province (in Chinese with English abstract). *Geoscience* 13:51–56
- Luo ZH, Ke S, Cao YQ, Deng JF, Zhan HW (2002) Late Indosinian mantle-derived magmatism in the East Kunlun (in Chinese with English abstract). *Geol Bull China* 21:292–297
- Macpherson CG, Dreher ST, Thirlwall MF (2006) Adakites without slab-melting: high pressure differentiation of island arc magma, Mindanao, the Philippines. *Earth Planet Sci Lett* 243:581–593. doi:10.1016/j.epsl.2005.12.034
- Maniar PD, Piccoli PM (1989) Tectonic discrimination of granitoids. *Geol Soc Am Bull* 101:635–643. doi:10.1130/0016-7606(1989)101<0635:TDOG>2.3.CO;2
- Martin H (1999) Adakitic magmas: modern analogues of Archean granitoids. *Lithos* 46:411–429. doi:10.1016/S0024-4937(98)00076-0
- Martin H, Smithies RH, Rapp R, Moyen J-F, Champion D (2005) An overview of adakite, tonalite-trondhjemite-granodiorite (TTG). *Lithos* 79:1–24. doi:10.1016/j.lithos.2004.04.048
- Mason DR, McDonald JA (1978) Intrusive rocks and porphyry copper occurrence of the Papua New Guinea-Solomon Island region: a reconnaissance study. *Econ Geol* 73:857–877
- Matte P, Tapponnier P, Arnaud N, Bourjot L, Avouac JP, Vidal P et al (1996) Tectonics of Western Tibet, between the Tarim and the Indus. *Earth Planet Sci Lett* 142:311–330. doi:10.1016/0012-821X(96)00086-6
- McCarthy TC, Patiño Douce AE (1997) Experimental evidence for high-temperature felsic melts formed during basaltic intrusion of the deep crust. *Geology* 25:463–466. doi:10.1130/0091-7613(1997)025<0463:EEFHTF>2.3.CO;2
- Müntener O, Kelemen PB, Grove TL (2001) The role of H₂O during crystallization of primitive arc magmas under uppermost mantle conditions and genesis of igneous pyroxenites: an experimental study. *Contrib Mineral Petrol* 141:643–658
- Nitoi E, Munteanu M, Marincea S, Paraschivoiu V (2002) Magma-enclave interactions in the East Carpathian subvolcanic zone, Romania: petrogenetic implications. *J Volcanol Geotherm Res* 118:229–259. doi:10.1016/S0377-0273(02)00258-5

- Pan YS, Zhou WM, Xu RH, Wang DA, Zhang YQ, Xie YW et al (1996) Geological characteristics and evolution of the Kunlun mountains region during the early Paleozoic. *Sci China Ser D* 39:337–347
- Pan GT, Ding J, Wang LQ, Zhuang YX, Wang QH, Zhai YG et al (2002) Important new progress of regional geological investigation in the Tibetan Plateau. *Geol Bull China* 21:787–793 in Chinese with English abstract
- Patiño Douce AE (1999) What do experiments tell us about the relative contributions of crust and mantle to the origin of granitic magmas? In: Carstro A, Fernandez C, Vigneresse JL (eds) Understanding granites: integrating new and classic techniques, vol 168. Geological Society, London, Special Publications, pp 55–75
- Peacock SM, Rushmer T, Thompson AB (1994) Partial melting of subducting oceanic crust. *Earth Planet Sci Lett* 121:224–227. doi:10.1016/0012-821X(94)90042-6
- Perermann M, Hirschmann MM (2003) Anhydrous partial melting experiments on MORB-like eclogite: phase relations, phase compositions and mineral—melt partitioning of major elements at 2–3 GPa. *J Petrol* 44:2173–2201. doi:10.1093/petrology/egg074
- Plá Cid J, Nardi LVS, Campos CS, Gisbert PE, Merlet C, Conceição H et al (2007) La, Ce, Nd, and Sr behavior in minette magmas during crystallization of apatite-clinopyroxene-mica paragenesis at upper-mantle conditions. *Eur J Mineral* 19:39–50. doi:10.1127/0935-1221/2007/0019-0039
- Popov VS, Boronikhin VA, Gmyra VG, Semina VA (1982) Garnets from the andesite-dacites of the Kel'sk volcanic highlands (Greater Caucasus). *Int Geol Rev* 24:577–584
- Prowatke S, Klemme S (2006) Trace element partitioning between apatite and silicate melts. *Geochim Cosmochim Acta* 70:4513–4527. doi:10.1016/j.gca.2006.06.162
- Qian ZZ, Hu ZG, Li HM (2000) Petrology and tectonic environment of Indosinian Hypabassal rock in the middle belt of East Kunlun Mountains. *J Mineral Petrol* 18:14–18
- Rapp RP, Watson EB, Miller CF (1991) Partial melting of amphibolite/eclogite and the origin of Archean trondhjemites and tonalites. *Precambrian Res* 51:1–25
- Rapp RP, Shimizu N, Norman MD, Applegate GS (1999) Reaction between slab-derived melts and peridotite in the mantle wedge: experimental constraints at 3.8 GPa. *Chem Geol* 160:335–356. doi:10.1016/S0009-2541(99)00106-0
- Ren MH, Parker DF, White JC (2003) Partitioning of Sr, Ba, Rb, Y, and LREE between plagioclase and peraluminous silicic magma. *Am Mineral* 88:1091–1103
- Richards J, Kerrich R (2007) Adakite-like rocks: their diverse origins and questionable role in metallogenesis. *Econ Geol* 102:537–576. doi:10.2113/gsecongeo.102.4.537
- Rodríguez C, Sellés D, Dungan M, Langmuir C, Leeman W (2007) Adakitic dacites formed by intracrystalline crystal fractionation of water-rich parent magmas at Nevado de Longaví Volcano (36.2°S; Andean Southern Volcanic Zone, Central Chile). *J Petrol* 48:2033–2061. doi:10.1093/petrology/egm049
- Rudnick RL, Gao S (2004) Composition of the continental crust. In: Holland HD, Turekian KK (eds) Treatise on geochemistry, vol 3. The Crust. Elsevier, Amsterdam; Pergamon, New York, pp 1–64
- Rushmer T (1991) Partial melting of two amphibolites: contrasting experimental results under fluid-absent condition. *Contrib Mineral Petrol* 107:41–59. doi:10.1007/BF00311184
- Schmidt MW (1992) Amphibole composition in tonalite as a function of pressure—an experimental calibration of the Al-in-hornblende barometer. *Contrib Mineral Petrol* 110:304–310. doi:10.1007/BF00310745
- Schulze DJ, Valley JR, Bell DR, Spicuzza MJ (2001) Oxygen isotope variations in Cr-poor megacrysts from kimberlite. *Geochim Cosmochim Acta* 65:4375–4384. doi:10.1016/S0016-7037(01)00734-7
- Schwab M, Ratschbacher L, Siebel W, McWilliams M, Minaev V, Lutkov V et al (2004) Assembly of the Pamirs: age and origin of magmatic belts from the southern Tien Shan to the southern Pamirs and their relation to Tibet. *Tectonics* 23:TC4002. doi:10.1029/2003TC001583
- Sen C, Dunn T (1994) Dehydration melting of a basaltic composition amphibolite at 1.5 and 2.0 GPa: implication for the origin of adakites. *Contrib Mineral Petrol* 117:394–409. doi:10.1007/BF00307273
- Sengör AMC (1987) Tectonics of the Tethysides: Orogenic Collage Development in a Collisional Setting. *Annu Rev Earth Planet Sci* 15:213–244. doi:10.1146/annurev.ea.15.050187.001241
- Skjerlie KP, Johnston AD (1996) Vapour-absent melting from 10 to 20 kbar of crustal rocks that contain multiple hydrous phases: implications for anatexis in the deep to very deep continental crust and active continental margins. *J Petrol* 37:661–691. doi:10.1093/petrology/37.3.661
- Smithies RH (2000) The Archaean tonalite–trondhjemite–granodiorite (TTG) series is not an analogue of Cenozoic adakites. *Earth Planet Sci Lett* 182:115–125. doi:10.1016/S0012-821X(00)00236-3
- Sobel E, Arnaud N (1999) A possible middle Paleozoic suture in the Altyn Tagh, NW China. *Tectonics* 18:64–74. doi:10.1029/1998TC900023
- Steiger RH, Jäger E (1977) Subcommission on geochronology: convention on the use of decay constants in geo- and cosmochronology. *Earth Planet Sci Lett* 36:359–362. doi:10.1016/0012-821X(77)90060-7
- Stern RJ (2002) Subduction zones. *Rev Geophys* 40:1012. doi:10.1029/2001RG000108
- Sun SS, McDonough WF (1989) Chemical and isotopic systematics of oceanic basalts: implications for mantle composition and processes. In: Saunders AD, Norry MJ (eds) Magmatism in the Ocean Basin, Geological Society Special Publication, vol 42. Blackwell, Oxford, pp 313–346
- Tassara A (2006) Factors controlling the crustal density structure underneath active continental margins with implications for their evolution. *Geochem Geophys Geosyst* 7:Q01001. doi:10.1029/2005GC001040
- Tatsumi Y, Eggins S (1995) Subduction Zone Magmatism. Blackwell, Oxford, pp 1–210
- Taylor HP Jr, Epstein S (1962) Relationships between $^{18}\text{O}/^{16}\text{O}$ ratios in coexisting minerals of igneous and metamorphic rocks: Part I. Principles and experimental results. *Geol Soc Am Bull* 73:461–480. doi:10.1130/0016-7606(1962)73[461:RBORIC]2.0.CO;2
- Taylor SR, McLennan SM (1985) The continental crust: its composition and evolution. Blackwell, Oxford
- van Sestrenen W, Blundy JD, Wood BJ (2001) High field strength element/rare element fractionation during partial melting in the presence of garnet: implications for identification of mantle heterogeneities. *Geochem Geophys Geosyst* 2:2000GC000133
- Wang GC, Wang QH, Jian P, Zhu YH (2004) Zircon SHRIMP P ages of Precambrian metamorphic basement rocks and their tectonic significance in the eastern Kunlun Mountains, Qinghai Province, China. *Earth Sci Front* 11:481–490
- Wang GC, Zhang TP, Liang B, Chen NS, Zhu YH, Zhu J, Bai YS (1999) Composite ophiolitic mélange zone in central part of eastern section of Eastern Kunlun Orogenic Zone and geological significance of “Fault belt in Central part of Eastern of Eastern Kunlun Orogenic Zone”. *Earth Sci J China Univ Geosci* 24:129–133
- Watson EB, Harrison TM (1983) Zircon saturation revisited: temperature and composition effects in a variety of crustal magma types. *Earth Planet Sci Lett* 64:295–304. doi:10.1016/0012-821X(83)90211-X

- Williams IS (1998) U–Th–Pb geochronology by ion microprobe. In: McKibben MA, Shanks WC, Ridley WI (eds) Applications of microanalytical techniques to understanding mineralizing processes. *Rev Econ Geol* 7:1–35
- Wu J, Lan CL, Li JL (2005) Geochemical characteristics and tectonic setting of volcanic rocks in the Muztag ophiolitic mélange, East Kunlun Mountains, Xinjiang, China (in Chinese with English abstract). *Geol Bull China* 24:1157–1161
- Xiao WJ, Windley BF, Chen HL, Zhang GC, Li JL (2002a) Carboniferous-Triassic subduction and accretion in the western Kunlun, China: implications for the collisional and accretionary tectonics of the northern Tibetan plateau. *Geology* 30:295–298. doi:10.1130/0091-7613(2002)030<0295:CTSAAI>2.0.CO;2
- Xiao WJ, Windley BF, Hao J, Li JL (2002b) Arc-ophiolite obduction in the Western Kunlun Range (China): implications for the Palaeozoic evolution of central Asia. *J Geol Soc Lond* 159:517–528
- Yang JS, Wu CL, Shi RD, Li HB, Xu ZQ, Meng FC (2002) Miocene and Pleistocene shoshonitic volcanic rocks in the Jingyuhu area, north of the Qinghai-Tibet Plateau. *Acta Petrol Sin* 18:161–176
- Yang JZ, Shen YC, Li GM, Liu TB, Zeng QD (1999) Basic features and its tectonic significance of Yaziqian ophiolite belt in eastern Kunlun orogenic belt, Xinjiang (in Chinese with English abstract). *Geoscience* 13:309–314
- Yin A, Harrison TM (2000) Geologic evolution of the Himalayan–Tibetan Orogen. *Annu Rev Earth Planet Sci* 28:211–280. doi:10.1146/annurev.earth.28.1.211
- Yin HF, Zhang KX (1997) Characteristics of the eastern Kunlun orogenic Belt. *Earth Sci J China Univ Geosci* 22:339–342
- Yu N, Jin W, Ge WC, Long XP (2005) Geochemical study on Peraluminous granite from Jinshuikou in East Kunlun (in Chinese with English abstract). *Glob Geol* 24:123–128
- Yuan C, Sun M, Zhou MF, Xiao WJ, Zhou H (2005) Geochemistry and petrogenesis of the Yishak volcanic sequence, Kudi ophiolite, West Kunlun (NW China): implications for the magmatic evolution in a subduction zone environment. *Contrib Mineral Petrol* 150:195–211. doi:10.1007/s00410-005-0012-0
- Zhang HF, Sun M, Zhou XH, Fan WM, Zhai MG, Yin JF (2002) Mesozoic lithosphere destruction beneath the North China Craton: evidence from major, trace element, and Sr–Nd–Pb isotope studies of Fangcheng basalts. *Contrib Mineral Petrol* 144:241–253